IN-BEAM GAMMA-RAY SPECTROSCOPY WITH THE HEAVY-ION REACTION ^{7}Li + ^{82}Se AT 35 MeV

A Thesis Presented to the
School of Graduate Studies
Addis Ababa University

In Partial Fulfilment
of the Requirement for the Degree
of Master of Science in Physics

By
Dagnachew Walelign

June, 1995

Dedication

The work is totally dedicated to my father Ato Walelign Workie and my mother W/o Yneayehu Melis for educating their children.

Acknowledgment

I am greatly indebted to my advisor Dr. Siegfried Tesch for his encouragement and continuous help throughout the work.

I gratefully acknowledge Dr.Georg Winter and his spectroscopy group at the Forschungszentrum Rossendorf for providing the data and information about modern trends in gamma-ray spectroscopy. My thank also goes to the Nuclear Data Section of the IAEA for providing the analysis software package GANAAS.

I wish to thank Ato Kebede Batu, General manager of National Scientific Equipment Center (NSEC), for his permission to use their NaI gamma-ray spectrometer which gave me basic understanding of gamma-ray spectroscopy. I would like also to express my indebtedness to Ato Mulugeta Desta and Ato Zewdu Bogale who are working in the Nuclear Instrumentation Unit of the NSEC for familiarizing me with the spectrometer.

I wish to thank Dr. Fesseha Kassahun, head department of physics, for his follow up and encouragement.

My acknowledgment also goes to Dr. S. Kotelinkov for formatting the data. I must also express my thanks to Ato Shewaferaw Solomon for helping to analyze some parts of the data. I also thank Ato Mesfin Tsige, who is currently at ICTP, for sending copies of related literature. With a great sense of debt, I thank Ato Wondwessen Mengesha, Ato Hailu Wolde and Ato Selemon Bekele for many useful discussions.

I would like also to express my sincere appreciation to all my friends whose continuous encouragement and moral support helped me towards the completion of the work.

I also thank the school of graduate studies for its financial support.

Contents

List of Tables

Page

List of Figures

Page

Abstract

The development of powerful heavy-ion accelerators and multi-detector systems had a strong impact on γ-ray spectroscopy. Via heavy-ion fusion-evaporation reactions one can produce very high-spin nuclear states. The highly excited nuclei then emit generally a large number of γ-rays, and the spectrum measured is a combination of different nuclear reaction channels. Consequently, γ-ray singles spectra are too complicated to identify transitions at high spin which are usually weak. Therefore, multi-detector with high resolution, good detector response and good efficiency are required to investigate such spectra. Some of the multi-detector arrays are therefore discussed in this work.

With the help of multi-detector systems high-spin states of nuclei have been studied in different mass regions. The mass $A \approx 80$ region is one of them where a number of interesting features have been observed, and this work is also devoted to this region. Hence, experimental and theoretical reviews of this mass region is included.

In the data analysis part a singles spectrum obtained from an in-beam measurement at 90^0 via the $^7Li + {}^{82}Se$ fusion-evaporation reaction at 35 MeV is analyzed with the software package GANAAS. The energies and intensities of γ-lines of selected nuclei obtained from GANAAS fits are compared with published data, and most of the lines that are accessible from the singles spectrum are found to be in a good agreement with other results.

Introduction

High-spin states in nuclei have been investigated extensively during the last years, and a lot of interesting phenomena have been observed. Fascinating progress in this new field has been made possible by the essential developments on exciting and detecting the high spin states in nuclei. Several types of nuclear reactions and processes have been explored to search for the best way of transferring a large amount of angular momentum to the final nuclear system. Such a transfer can be expected in nuclear reactions initiated by energetic heavy-ion (HI), $A \geq 4$, projectiles. Fusion reactions and multiple Coulomb excitation have appeared to provide most efficient ways of populating high-spin states.

After the compound nucleus is formed, an equilibration process distributes the energy over all nucleons, some of which can be emitted. Mostly, several neutrons are emitted from such a highly excited nucleus. In general, not only neutrons but also charged particles can be emitted from a highly excited nucleus. A state populated by a particle that is emitted last is called an entry state. The set of all entry states forms the entry region. The γ-radiation emitted is composed of discrete and continuum γ-rays. In the discrete energy region, at low excitation energy, the level density is low enough to enable observation of electromagnetic transitions as resolved lines in the γ-ray spectrum. With increasing excitation energy, however, the level density increases, creating many pathways for the γ-rays which constitute a " continuum " in the spectrum.

With the possibility of studying experimentally very high-spin states using HI beams, new techniques have been developed to detect the de-exciting γ-rays. Enhancement of those γ-rays with respect to the background has been achieved by using multi-detector systems.

Simultaneously with the vast increase of experimental data on high angular phenomena a certain level of understanding has been achieved in the structure of the underlying nuclear motion. The nuclear motion is characterized by an intimate interplay of collective and single-particle degrees of freedom.

The first extreme to produce angular momentum is collective rotation. In this case many - if not all - nucleons participate in the collective process. That is, the rotational motion involves coherent contributions from many nucleons. Each nucleon carries a small angular momentum and all these small amounts add up to the total angular momentum, which can be very large. This type of motion is observed for deformed nuclei, i.e. those characterized by a non-spherical spatial distribution of the nuclear density. A schematic example of a prolate nucleus rotating around an axis perpendicular to the nuclear symmetry axis is shown in Fig.I.(a) (see [Twi89]).

Fig. I. Two different modes of rotation generating angular momentum. (a) Collective rotation of a prolate nucleus, (b) particle alignment in an oblate nucleus.

The second mechanism, the single-particle motion, is likely to exist in spherical or weakly deformed nuclei. Here the alignment in the individual nucleonic orbitals along the nuclear symmetry axis appears to be the only possible mechanism of building up the high angular momentum. This type of motion (often referred to as a non-collective rotation) is illustrated schematically in Fig.I.(b). In this case a few valence nucleons move in an oblate averaged potential and populate orbitals with positive angular momentum projections on the symmetry axis. Since the density distribution of aligned configurations is maximal in the plane perpendicular to the angular momentum axis, one obtains for valence particles slightly oblate shapes with the symmetry axis parallel to the angular momentum.

The different types of rotation, and the corresponding shapes, can be recognized experimentally from the level scheme of the nuclei. In the case of collective rotation the spacing between the levels has a regular sequence. Therefore, the excitation energy E^* and the spin I is often a smooth one and, for spins that are not too high, E^* can be approximated by $E^* \sim I\ (I + 1)$. The corresponding states with increasing angular momentum are called rotational bands. The lowest energy of a given angular momentum is called the yrast state. The sequence of all yrast states (represented in the E^* vs I plane) is called the yrast line. One such example having regular sequences of states is ^{168}Hf [Cha83]. In contrast, for single-particle rotation the decay scheme is irregular and complicated by isomeric states. Excitation energy and angular momentum are generated by single-particle motion; therefore, the corresponding yrast sequence is characteristic of a system that continuously changes its configuration. The resulting yrast energy spectrum represented as a function of angular momentum forms a considerably irregular sequence – no $I\ (I + 1)$- rule obeyed locally. However, the yrast line produced by such non-collective rotation obeys on the average an $I\ (I + 1)$ rule over a large interval of angular momentum. For example, one such type of nucleus exhibiting an irregular decay scheme is ^{147}Gd [Bak82].

Certainly, collective and non-collective (or single-particle) rotations are only extreme cases. Both structures can coexist in the same nucleus, and most nuclei combine both types of motion. It is this interplay between collective and single-particle motion that makes the behaviour of nuclei along the angular momentum co-ordinate so fascinating and so rich in variety. A typical example exhibiting both types of motion is ^{152}Dy [Kho78]. At very high angular momentum the difference between the two excitation modes becomes less and less pronounced, since at very high spin all orbitals tend to align their angular momenta completely, regardless of the kind of rotation.

The aim of this work, in addition to reviewing the in-beam gamma-ray spectroscopic studies of the mass $A \approx 80$ region, is to analyze data obtained in an in-beam measurement via the fusion-evaporation reaction ^{7}Li + ^{82}Se. The singles spectrum of γ-lines obtained with a single Ge-detector is compared with those obtained using an array of detectors. The software package used to analyze the spectrum is GANAAS (Gamma Spectrum Analysis, Activity Calculations and Neutron Activation Analysis).

The first section describes some important in-beam γ-ray measurements using beams of heavy ions. Detector requirements to push discrete γ-line studies to high spins and different multi-detector arrays in order to meet this requirements and present trends of in-beam γ-ray spectroscopy is discussed in this section. De-excitation processes of highly-excited nuclei are described in section two. The third section deals with the results of an in-beam γ-ray spectroscopic study in the mass $A \approx 80$ region. Experimental and theoretical findings, such as high spins and large deformation, in this mass region are discussed here. The fourth section is devoted to the analysis of the γ-spectrum obtained in an in-beam measurement of the reaction ^{7}Li + ^{82}Se. Comparison and discussion of γ-lines with published data is done in this section. Finally, conclusions are drawn from the results of the data analysis.

1. Experimental Review of In-Beam Gamma-Ray Spectroscopy

1.1. Methods of In-Beam Gamma-Ray Spectroscopy With Heavy Ions

The aim of in-beam γ-ray spectroscopy is the measurement of the characteristics of γ-rays emitted in nuclear reactions, the deduction of the properties of nuclear levels, the determination of the nature of excited states, and finally comparison with theory. To do this one has to carry out various measurements on the γ-rays. In the present section we will discuss some of the methods used in nuclear-structure and reaction mechanism studies.

Excitation Functions. In a HI fusion-evaporation reaction, as a result of the emission of different particles we get various final products. Therefore, the study of excitation functions for each reaction channel is important. The energy dependence of the cross-section for any specific nuclear reaction, for instance-A (HI, Xn) B, is called excitation function. If these functions are known, one can select the incidence energy in order to remove the number of open reaction channels, or the cross-section of one or a few reactions are at maximum, while other channels are strongly suppressed. This way one is able to reduce the complexity of the γ-ray spectra obtained in the in-beam measurements [Joh75].

A higher energy of the projectile also results a transfer of larger angular momentum and shifts the spin distribution of the final nucleus to higher spin values. The feeding into the yrast states will therefore occur at higher spin values and transitions between high-spin states will become more frequent than low-lying transitions. A comparison of the change of the relative intensities of transitions attributed to a certain nucleus as a function of projectile energy can therefore indicate the spin values involved [Joh75].

Angular Distributions. In a compound-nuclear reaction the projectile brings orbital angular momentum to the compound nucleus. Taking the beam direction as the axis of quantization, for spherical target only m = 0 states will be populated, i.e. the total angular momentum vector of the compound nucleus is aligned in a plane perpendicular to the beam direction. Deviations may arise from the spins of the projectile and the target nuclei. The emitted neutrons carry away only a few units of angular momentum (sec. 2.3). The neutron evaporation process will influence the initial alignment only slightly and just cause a small broadening of the population of the m-state. The γ-rays emitted from the final nucleus show characteristic angular distributions with respect to the beam axis, which can be used to determine the multipolarity of the emitted γ-rays.

Lifetime Measurements. Many different techniques have been developed in order to measure lifetimes of excited states in various time range [Fen86]. For lifetimes larger than about 1-3 ns, well-defined beam pulses from an accelerator can be used for lifetime measurements. A cyclotron, for example, can be designed so as to produce a pulsed beam with ~ 100 ns (100 MHz) between the pulses, with a FWHM of about 1-3 ns.

The majority of the nuclear levels that decay by γ-ray emission have lifetimes of the order 10^{-14}s to 10^{-9}s. This time region is experimentally covered by two methods, namely the Doppler-shift attenuation method (DSAM) and the recoil-distance method (RDM). These methods cover the time range $10^{-14}\text{s} \leq \tau \leq 10^{-11}\text{s}$ and $10^{-12}\text{s} \leq \tau \leq 10^{-9}\text{s}$, respectively [Pel82]. The main difference between the RDM and the DSAM is the time scale to which the nuclear lifetimes are compared. In the RDM the time scale is established by means of the time the excited nuclei with speed v need to travel over a certain distance (where they are stopped in times short compared to the flight). In the DSAM the nuclear lifetime is compared to the time in which the excited nucleus with initial speed v is slowed down in solid material. Both techniques are based on the Doppler effect. That is, the γ-rays emitted from a moving nucleus will have an energy shift given by, considering only the first order terms in v/c,

$$E_\gamma = E_{\gamma 0}(\,1 + \frac{v}{c}\cos\theta\,), \tag{1.1}$$

where E_γ is the shifted γ-ray energy, $E_{\gamma 0}$ is the energy of γ-ray emitted by a nucleus at rest, c is the velocity of light, θ is the angle of γ-ray emission relative to the recoil direction. How the two methods are used for lifetime measurements is discussed in the following paragraphs.

Important components of the apparatus used in RDM measurements are the target and the stopper which are usually positioned perpendicular to the beam direction and which are separated from each other by a distance d. The target has to be thin enough for nuclei produced in the target to recoil into vacuum. The intensity I_F of the γ-ray with Doppler-shifted energy and the intensity I_S of the γ-rays emitted after the nuclei are stopped are related to the distance d, for a pure radioactive decay with lifetime τ , by

$$I_F(d) = I_0[\,1 - \exp(-\frac{d}{v\tau}) \tag{1.2}$$

and

$$I_S(d) = I_0\exp(-\frac{d}{v\tau} \;, \tag{1.3}$$

where $I_0 = I_S + I_F$ is the total number of γ-rays emitted. The ratio R between the stopped intensity I_S and the total intensity I_0 is

$$R(d) = \exp(-\frac{d}{v\tau}) = \exp(-\frac{t_F(d)}{\tau} , \qquad (1.4)$$

where $t_F = d/v$ is the flight time. Thus the measurement of R(d) as a function of d allows τ to be determined if τ is of the order of t_F.

On the other hand, nuclear lifetimes of the order of $10^{-14}s \leq \tau \leq 10^{-11}s$ can be determined by means of the DSAM. The method basically consists of comparing the nuclear lifetime with the time in which a nucleus is stopped in solid material. The γ-rays that are emitted during the slowing down process, i.e. at times smaller than the stopping time, say $t_S(v)$, are shifted in their energy according to Eq.(1.1). On the other hand, all nuclei decaying at times $t \geq t_S(v)$, will contribute to an unshifted line at $E_\gamma = E_{\gamma 0}$. Thus in case a nucleus in a particular state is produced at time t = 0 with well defined initial velocity v, the ratio of the intensity of the unshifted line to the total intensity is given by

$$R(v) = \exp(-\frac{t_S(v)}{\tau}), \qquad (1.5)$$

which allows to determine its lifetime τ if $t_S(v)$ is known and of the order of τ. Depending on the stopping material and the initial recoil velocity the stopping times range from 5×10^{-12}s to 5×10^{-13}s [Pel82].

γ-γ Coincidence Measurements. The first problem to be solved in discrete γ-ray spectroscopy using HI reactions is to enhance the transitions to be studied by suppressing unwanted reaction channels and by selecting the gamma cascades of interest. The usual and certainly the cleanest method is to perform γ-γ coincidences measurements employing two or more Ge-detectors and to record γ-spectra in coincidence with one of the characteristic transitions in the residual nucleus. Thereby one does not only prove that a certain γ-ray belongs to the decay scheme of the residual nucleus, one simultaneously selects those cascades feeding and depopulating the states connected by the gating transition, which is an important prerequisite to place the γ-lines in the level scheme.

Therefore, the stronger argument for a certain level structure is normally based on γ-γ coincidence measurements [Pel82]. By studying the relative intensities in the coincidence spectra, the position of the excited states in the sequence can be established.

1.2. Detector Requirements and Solutions for In-Beam Measurements

The advent of powerful heavy-ion accelerators had a strong impact on gamma-ray spectroscopy. In heavy-ion reactions one can produce nuclei in states carrying very high angular momenta. The nuclei emit generally a large number of γ-rays in order to get rid of the excitation energy and angular momentum it acquires during the heavy-ion collision. Furthermore, a large number of residuals with comparable cross-sections will be formed. Consequently, the γ-ray spectra are very complex. On the other hand, nuclear spectroscopic studies were often limited by either insufficient energy (or time) resolution or insufficient statistics, or both. Recently high-resolution and high-statistics γ-ray systems have become available in order to push discrete γ-line work to high spins [Twi89, Dia86]. The primary requirements for high-spin studies are high energy resolution, good detector response, and good efficiency. Some solutions for these requirements are discussed in the following paragraphs.

Lithium-drifted or intrinsic germanium detectors are now commercially available providing the highest energy resolutions of 1.5-2.0 keV at 1.0 MeV and photo peak efficiencies of more than 30% relative to a 3" X 3" NaI(Tl) detector. The high energy resolution of Ge-detectors is particularly important for in-beam measurements where the spectra are usually too complicated. In contrast to the measurements with NaI-detectors, measurements with Ge-detectors isolate most of the lines even in such spectra (Fig. 1.1)

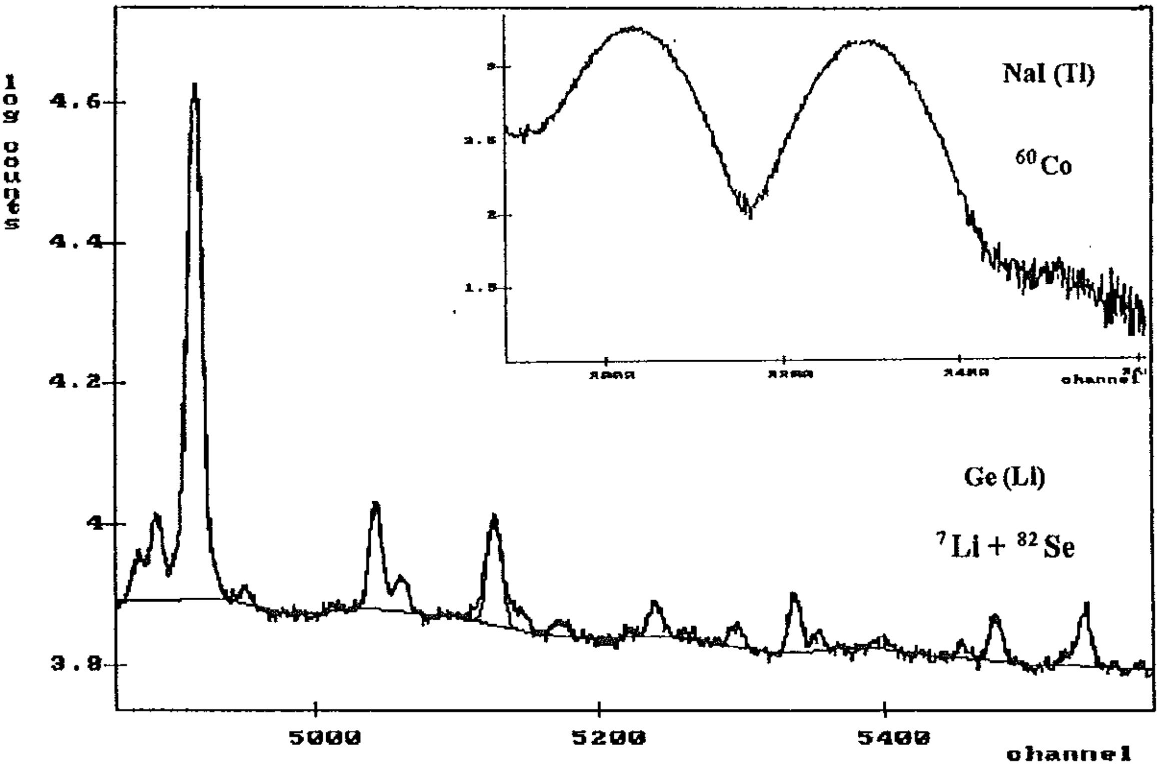

Fig. 1.1. Comparison of an in-beam spectrum from the reaction ^{7}Li + ^{82}Se measured with a Ge-detector and the ^{60}Co spectrum measured with a NaI detector. The energy interval in both cases is the same. The line below the peaks is the fitted background.

Ge-detectors cover the energy range from typically 50 keV to several MeV photon energy, while γ-ray transitions of still lower energy can be recorded in Li-drifted or intrinsic silicon detectors. Modern γ-ray systems are therefore based on array of such detectors . The reason to use an detector array is explained as follows. If two γ-rays fall nearly on the same point (within the 2 keV resolution), they can not be resolved by a single detector. The γ-rays obtained from fusion-evaporation reactions are usually not single events; rather they are members of a cascade and, therefore, are in coincidence with the other members. If two (or more) detectors are used, then coincidence measurement may serve to resolve them. The number of resolvable γ-lines can be increased by increasing the number of detectors. Therefore, it is always advantageous to use multi-detector arrangements as close as possible to the target, in order to favour higher-order coincidences so that effective resolution can be achieved. In addition, heavy-ion fusion-evaporation reactions are not very selective in the production of the final nucleus. Different final nuclei can be formed by evaporation of different particles, such as neutrons and protons, and the number of nucleons evaporated can vary. The use of a multi-detector system allows to select a specific channel [Twi89].

The second requirement is to have a good response, i.e., every γ-ray that strikes the detector should result in an output signal proportional to the original γ-ray energy. A Ge-detector does not fulfill this requirement very well. The relatively low atomic number (Z = 32) and moderate density (5.33 g/cm^3) results mostly in Compton scattering. With a 5 x 5 cm Ge-detector (approximately 20% efficiency of a 7.6 x 7.6 cm NaI detector for 1.33 MeV γ-rays) a 1.33 MeV γ-ray has an absorption probability of ~ 3/4 and a peak to total (P/T) ratio of 15-20%. This means that ~ 1/4 of such γ-ray do not interact at all with the detector, and that of those that do, only 15-20% contribute to the full energy peak. In a double coincidence measurement, only 2-4 % of the events obtained are good full-peak events, the remaining 96-98% are unwanted garbage. This is a very undesirable situation. Therefore, modern γ-spectrometers use Compton-supression shields around the

Ge-detectors. For this purpose large NaI, say 20 x 25 cm, and/or BGO shields are applied. The material has a chemical formula $Bi_4 Ge_3O_{12}$.

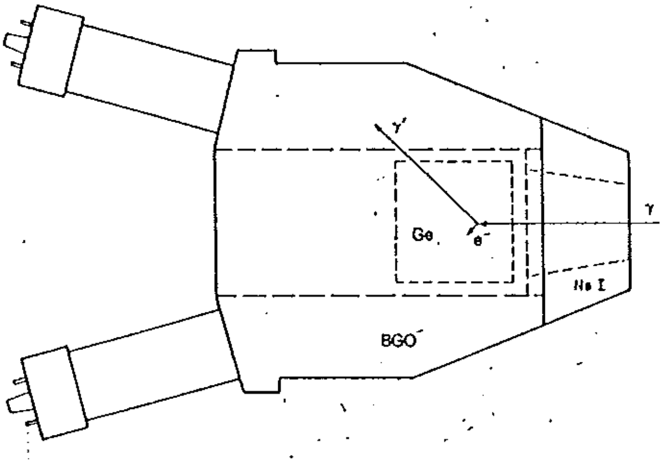

Fig. 1.2. Outline of the anti-Compton BGO shielded Ge-detector [Dia86]

The Compton scattered γ-ray, labeled γ', is lost if there is no shield surrounding the Ge-crystal (see Fig.1.2). If this shield is made of a scintillator which is sufficiently dense to stop γ', then the output of the photomultiplier tube gives a signal. This signal is essentially due to the Compton events originating in the Ge-detector. By putting this pulse produced by the scintillator shield in anti-coincidence with the Ge-detector signal it is possible to reject the Compton events produced in the Ge-detector. Therefore, only Ge-events in which there is no event in the shield are accepted. This gives a remarkable improved peak to total ratio. The scintillator used for such a shield has to be dense enough to stop the Compton-scattered γ-rays.

Instead of NaI shields bismuth germanate (BGO) shields are widely used. The BGO shield offers a great advantage over NaI. The material is considerably denser (7.13 g/cm^3) and of higher average Z , so that it has a γ-ray absorption length 2 1/2 times smaller than NaI (with density 3.67 g/cm^3). This means more compact shields, so that more Compton-supressed detectors can be placed near the target to measure higher-order coincidences with good statistics. Putting Compton-supression shields around the Ge-detectors helped to get a tremendous improvement in the Ge-detector response. To have some feeling how significant is the improvement [Dia86]: the peak to total ratio for ^{60}Co above a 300 keV threshold improves from ~ 20% with the bare Ge-detector to 50-70% with a BGO shield. For coincidence experiments this makes an enormous difference. For example, with bare Ge-detectors 20% of P/T ratio full energy triple coincidences are only 0.8% of the events, so that triple coincidences could not be measured with unshielded spectrometers. But with 50% P/T ratio, 12.5% are full-energy events, therefore, triple coincidence measurements can be done.

The system efficiency involves the question of how many Ge-detectors at what distance from the target should be placed. Minimizing the distance between the Ge-detectors and the target will increase the counting rates and hence the system efficiency. Good statistics is always vital, but if higher count rates are utilized, then care must be taken to identify and ignore signals which are amplitude shifted due to pile-up. A major signal-to-noise degradation can occur if the Ge-detectors are placed very close to the target in order to increase the solid angle and thus data rate. This will result in two unwanted effects; one is γ-ray summing in each individual detector; the other is an increase in the magnitude of Doppler broadening for detectors near 90° to the beam (product recoil) direction.

Doppler broadening must be considered for each nuclear system studied as the effect can be quite large in (HI, Xn) reactions, where the recoil velocity attains several percent the speed of light. For example, in a typical case , ~ 180 MeV ^{40}Ar on ^{124}Sn, the recoiling compound nucleus has a velocity ~ 2.5% that of light. The first order Doppler shift for a γ- ray emitted by such a moving source is given by Eq.(1.1). So for θ near 0^0 or 180^0 the Doppler shifts are quite large, 25 keV for a 1 MeV γ-ray (for our reaction, 35 MeV ^{7}Li on ^{82}Se, the corresponding Dopler shift is about 3 keV). But the Doppler broadening due to the finite opening half-angle ϕ of the detector [Dia86]

$$\frac{\Delta E}{E_o} = 2\frac{v}{c}\sin\theta\sin\phi \qquad (1.6)$$

is quite small, $\leq$ 0.5 keV for $\phi = 9.5^0$. On the other hand, for angles of θ near 90^0 , the Doppler shift becomes small, but the broadening becomes a maximum (see Eqs.(1.1) and (1.6)). For the example, $\frac{\Delta E}{E_0} \cong 0.8$ % or 8 keV broadening for a 1 MeV line. Such a smearing of the energy ruins the resolution of the detector, but can be reduced or avoided altogether under certain conditions. For example, if such a product nucleus recoils out of the target into a lead or gold backing, it will stop within several picoseconds (ps). If the photons are emitted after stopping ($v = 0$), there will be no Doppler shift or broadening. Thus, nuclei that have some slow, mostly non-collective transitions in their de-excitation cascades can, and do, take picoseconds to de-excite and do not present a problem. But if the γ-transitions are fast, something has to be done to alleviate the Doppler broadening; the detector must be moved away from the detector, or a collimator must be used, or both, in order to decrease the detector opening angle, and thus broadening. However, since we would like also to increase the system efficiency the detectors positions should not be too far from the target. To reconcile these differences one has to try and find an optimum position, so that to get increased system efficiency and at the same time minimized Doppler broadening. Besides the continuing effort to improve the detection system, there are already different multi-detector arrays designed to help the different requirements and push discrete γ-line studies to high-spin states. Some of the multi-detector arrays are discussed in the next section.

1.3. Modern Trends of In-Beam Gamma-Ray Spectroscopy

All heavy-ion induced fusion-evaporation reactions end with different residual nuclei formed by evaporation of different number of particles. As a result the singles γ-spectra are very complicated. On the other hand, the study of the γ-decay from very high-spin states demands an instrument capable of selective detection of very weak γ-ray transitions. Therefore, a detailed study of the de-exciting γ-rays with common γ-spectrometers is very difficult or even impossible.

At present there are many multi-detector arrays used (or under construction) to study the details of such decay paths. The common objectives of these detection equipment is to fit the experimental requirements mentioned in the above section. The " Total Energy Suppression Shield Array " (TESSA) installed at the tandem accelerator laboratory at Daresbury has been the pioneer in this field. It combines high-resolution Ge-detectors, each

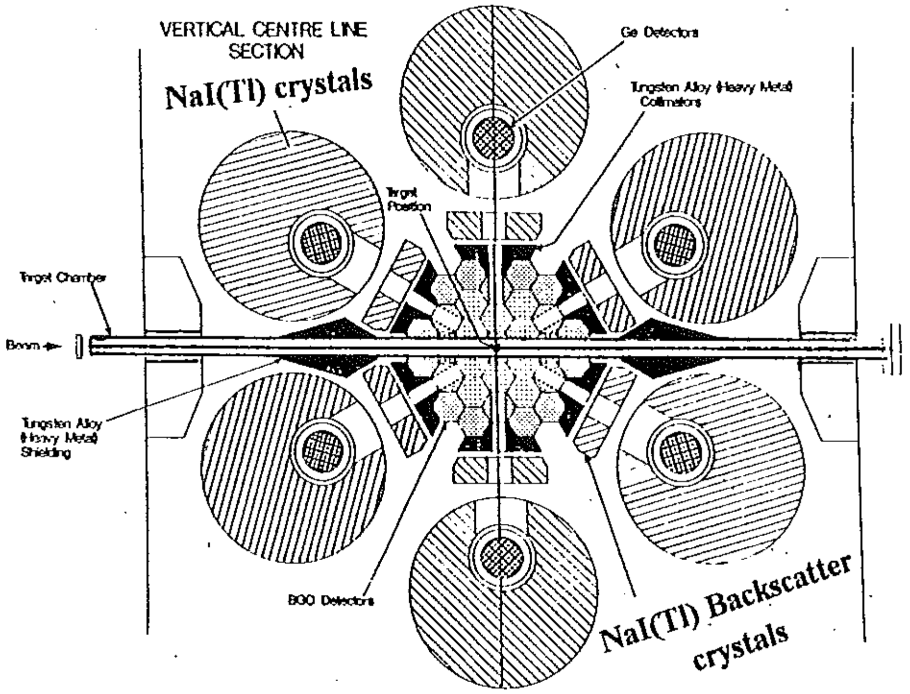

Fig. 1.3. Configuration of TESSA II. It consists of 6 Compton suppressed Ge-detectors and 62 BGO crystals of hexagonal cross-section [Twi83].

surrounded by a veto detector (suppression shield) of sodium iodide and/or bismuth germanate, and a compact bismuth germanate (BGO) ball (Fig.1.3). In this section TESSA is selected to describe some of the properties of multi-detector arrays [Twi83].

The suppression shields used in TESSA are 25 cm diameter by 20 cm long NaI-crystals with the Ge-detectors inserted parallel to the crystal axis. This geometry provides the best suppression at low γ-ray energies through efficient detection in the shield of the high energy forward scattered γ-rays.

The effect of such suppression is shown in Fig.1.4 for a ^{60}Co source. The dominant remaining feature are the backscatter peaks (Compton edges) close to 250 keV below the photo peaks. Fig.1.4(b) shows that these backscatter peaks are removed by the NaI backscatter detectors positioned as shown in Fig.1.3. The collimation of γ-rays striking the Ge-detectors is achieved by tungsten alloy (heavy metal) hexagons in the outer ring of the BGO-ball. They are designed so that γ-rays from the target are restricted to pass through a 4 cm diameter circle at the center of the Ge-detectors. This ensures good photo peak to

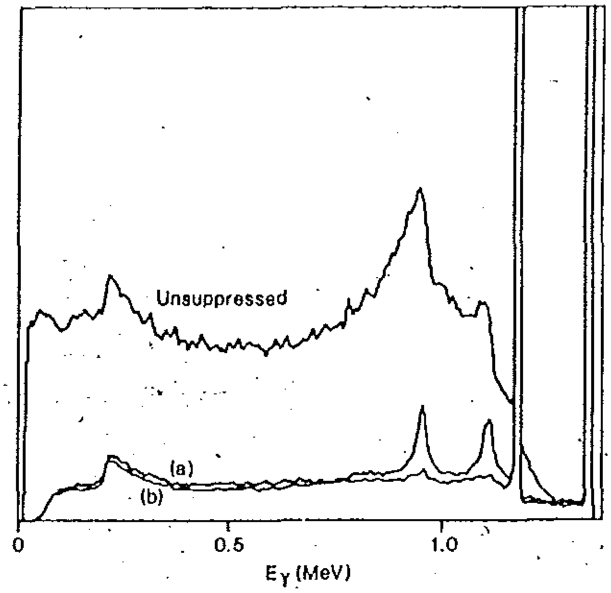

Fig. 1.4. The effect of suppression on 1.17 MeV and 1.33 MeV γ-rays from a ^{60}Co source; (a) veto by NaI-shield, (b) veto by NaI shield and backscatter detector [Twi83].

total fractions before suppression. The peak efficiency is increased from (15 − 20)% for a bare Ge-detector to (55 − 65)% for a Compton suppressed detector.

The center of the Ge-detectors are 27 cm from the target and their collimated solid angles are 0.16% each. The small solid angle is necessary to reduce Doppler smearing caused by the change in energy across the detector of γ-rays emitted from fast moving recoils and pile up caused from the detection of two γ-rays in the same Ge-detector due to the high multiplicity of events. The 6 Ge-detectors constitute 15 pairs thus increasing the γ-γ coincidence efficiency. In a typical HI reaction experiment with TESSA the Ge-detector singles rate is around 5000 s^{-1} and the γ-γ coincidence rate is about 150 s^{-1}. In γ-γ coincidence experiments the important quantity is the fraction of the recorded γ-γ events that are photo peak-photo peak events as the remainder just increases the Compton continuum. The suppression improves this fraction from 0.03 to 0.29 for 1.2 MeV γ-rays and from 0.1 to 0.42 for 0.66 MeV γ-rays [Twi86]. It is this big increase in the fraction of useful γ-γ coincidence data that greatly assists carrying out detailed spectroscopy on low intensity γ-ray branches.

An essential feature to improve the sensitivity of the TESSA ball is compactness. This means, a denser scintillator than NaI was necessary, and BGO was chosen. The BGO ball has been designed as a cylindrical and this allows to put the Compton suppressed Ge-detectors close to the target. Each BGO-crystal has a hexagonal cross-section with dimensions of 38 mm face to face and 50 mm or 75 mm in length. The 62-BGO detectors form a honeycomb arrangement which operates as an effective 50 detectors ball having an overall solid angle close to 4π, and this allows to absorb the transitions with large probability.

Though TESSA is the pioneer in this field, other improved multi-detector arrays are also operational in different countries. With the discovery of the superdeformation (nuclei with major to minor axis ratio 2:1) [Twi86] a renaissance in γ-ray spectroscopy has been started. Twin and co-workers used for the first time a spectrometer consisting of 12 Ge-detectors with Compton suppression. This new technique initiated a new generation of γ-spectrometers in Europe, USA, and Canada with 6 up to 20 Ge-detectors surrounded by compact BGO counters to suppress the Compton background. Among them are the 21 Compton suppressed Ge-detectors HERA (High-Energy Resolution Array) with 44 BGO counters at Berkeley, NORDBALL with 15 Compton suppressed Ge-detectors, 11 neutron detectors and a 4π Si-ball at Kopenhagen, CHATEAU DE CRISTAL at Strasbourg, and OSIRIS (Compton Suppression Array for High-Resolution In-beam Spectroscopy) having 38 BGO detectors and 12 Ge-detectors with BGO + NaI (Tl) shield of the Jülich / Berlin / Köln/ Bonn/ collaboration. Also, at Daresbury, the POLYTESSA array with 30 Ge-detectors having compact BGO + NaI(Tl) shields is currently taking data. This array is the result of contributions from the U.K.TESSA collaboration, the German OSIRIS collaboration, the Scandinavian NORDBALL collaboration and the Italian MIPAD collaboration.

With these spectrometers superdeformation could be found in many nuclei. However, the sensitivity was too low for a detailed γ-spectroscopy of superdeformed bands. Therefore, large collaborations started to build up 4π-spectrometers with improved properties of the detectors. The sensitivity of the detectors for the measurements of multiple coincidence events depends on solid angles seen by the Ge-detectors and the granularity of the whole array to keep low the line broadening due to the Doppler-effect and the probability for measuring coincident γ-rays in the same detector.

The American spectrometer GAMASPHERE will consist of 110 large-volume Ge-detectors with BGO-shield each in spherical geometry. Every detector has an efficiency of about 80% for the total absorption of γ-rays measured relative to a 3" x 3" NaI detector at energy of 1.3 MeV. The total efficiency of the spectrometer for the total absorption of the 1.3 MeV radiation is expected to be ~ 8%.

The European spectrometer EUROBALL will contain, in its final version, 270 Ge-detectors of a new generation. In this detector array a high granularity is envisaged to minimize Doppler broadening, and the total efficiency will be 13% for the 1.3 MeV γ-rays. This project will be realized in three phases.

Phase I have put two spectrometers-EUROGAM I and GASP - into operation in Daresbury (England) and Legnaro (Italy), respectively. Both spectrometers contain about 40 Ge-detectors with BGO Compton suppression shields. In phase II of this expensive project the granularity will be increased when using so-called CLOVER detectors [Ebe93] now under development. EUROGAM II will be installed at a new tandem-accelerator VIVITRON in Strasbourg. The final phase III of the EUROBALL project (see [Ger92]) is expected to reach a sensitivity of one order of magnitude higher than EUROGAM II (fraction of reaction ~ 2×10^{-6} for very weak γ-radiation). This high sensitivity is necessary to find the theoretically predicted hyperdeformation in nuclei with a ratio of the major to minor axes of 3:1

Improving the experimental technique enables to push discrete line studies to very high-spin states (see Fig.1.5). Using NaI-detectors one can reach only spins up to ~ 10$\hbar$ and using Ge- detectors discrete line studies can be pushed further up to ~ 20$\hbar$. The invention of the TESSA family has a strong impact in the field of in-beam γ-ray spectroscopic studies. For example, with the TESSA3 array high-spin states as high as ~ 60 ħ could be observed. At present the observational limit of high-spin states, using EUROGAM I, is around 70ħ. The prediction of the observational limit with EUROGAM II is around 75ħ.

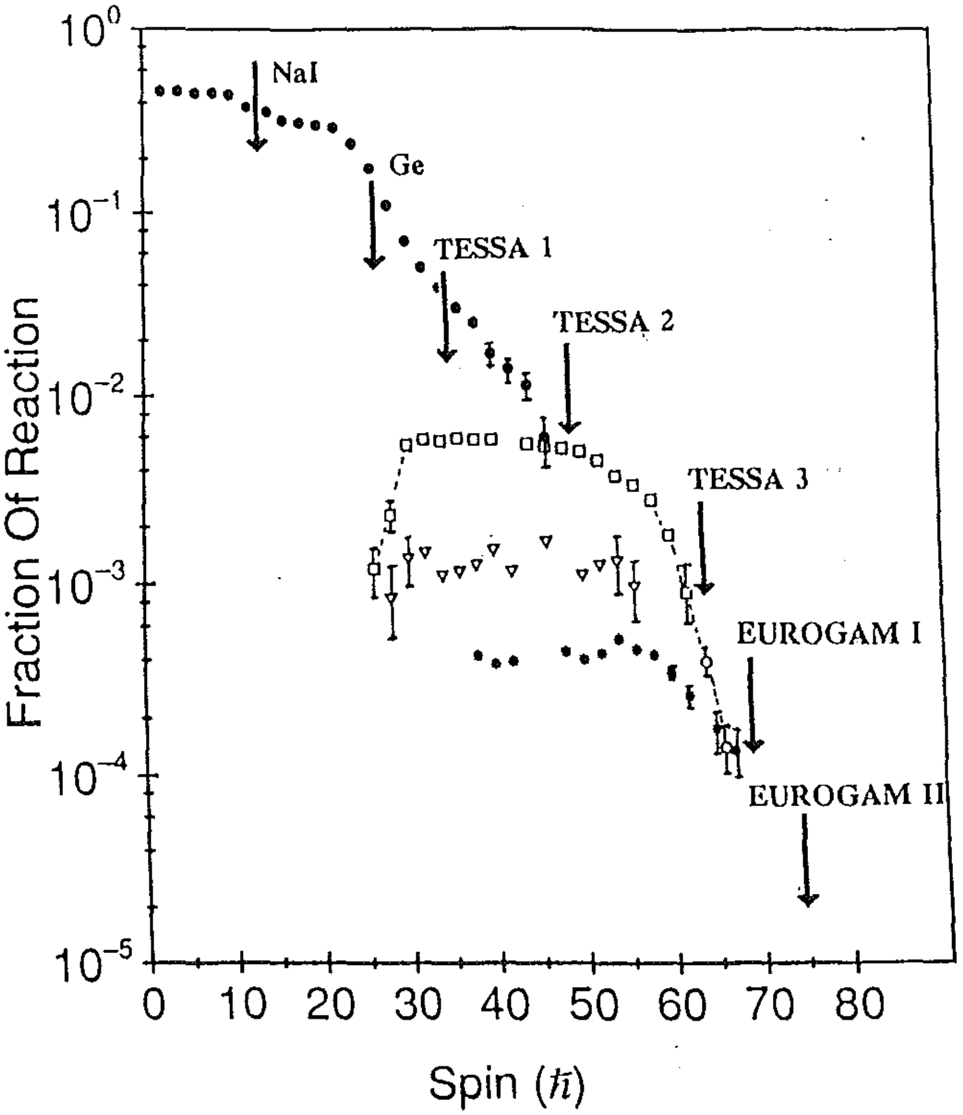

Fig. 1.5. Observational limits of γ-rays with different detection systems. The data points are: solid circle (•) discrete lines in ^{160}Er measured with TESSA2; open square (□) yrast superdeformed band in ^{152}Dy and open triangles (∇) first excited superdeformed (SD) band in ^{151}Tb measured with TESSA3; open circle additional γ-rays in the yrast SD band in ^{152}Dy and stars (*) excited superdeformed band in ^{152}Dy measured with EUROGAM I [Twi94].

2. Formation and Decay of Highly Excited Nuclei

2.1. General Features of Heavy-Ion Reactions

When a target is hit by a beam of heavy ions, A ≥ 4, three major classes of nuclear processes have been identified. For relatively large impact parameters and at bombarding energies below the Coulomb barrier Coulomb excitation and Rutherford scattering processes are in sole control. At bombarding energies slightly above the barrier and for relatively large impact parameters the cross-section for few-nucleon transfer reactions by tunneling can be considerable. The above processes may be referred to by the collective term of "barrier processes". With increasing energies of the incoming ions and at smaller impact parameters the projectile can penetrate the Coulomb barrier and the compound nucleus formation becomes dominant up to energies where the direct reaction mechanism with violent collision processes dominate (stripping, pick-up, etc.).

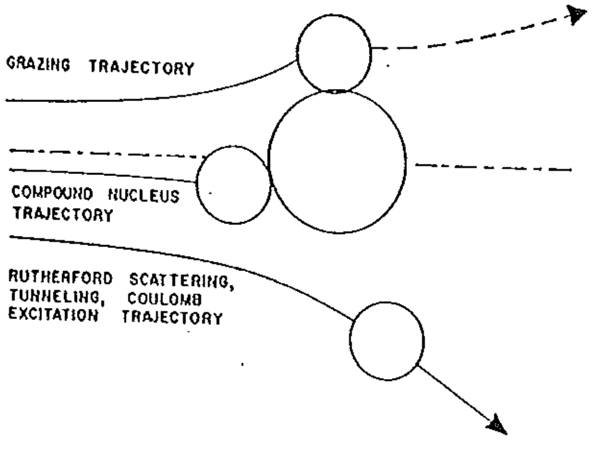

Fig. 2.1. Typical trajectories representing the three major classes of heavy-ion reactions [kau61].

The third type of nuclear reaction is observed at intermediate impact parameters for which the projectile, though partially deflected by the Coulomb field, comes into approximately tangential contact with the target nucleus (Fig. 2.1). It may then move along the surface of the target until it reaches a point at which its forward momentum is sufficient to break the nuclear bond formed between the nuclei. If this process is completed before fusion to a compound system, a grazing collision results [Boc89]. In this process the transfer of several nucleons can occur. The products of such an interaction are the residue of the projectile, the residue of the target, and perhaps free nucleons and alpha particles which may be emitted as the system separates.

The compound nucleus is a more or less deformed system consisting of all the impinging nucleons, often formed with high angular momentum and high excitation. It removes its excitation through successive particle emission followed by γ-ray cascades.

2.2. Cross-Section for the Formation of Compound Nuclei

According to Fig. 2.1 heavy-ion collisions at a fixed bombarding energy can be divided into different classes. One of these collision processes may lead to fusion of the projectile and the target nucleus forming a compound nucleus. That is, at smaller impact parameters and at bombarding energies only slightly above the Coulomb barrier the projectile can penetrate the Coulomb barrier, and a nuclear bond is then formed to form a compound system, which then decays in some subsequent time.

In heavy-ion collisions the total nuclear reaction cross-section is given by the expression

$$\sigma_R = \pi \bar{\lambda}^2 \sum_{l=0}^{\infty} (2l + 1)^2 T_l, \tag{2.1}$$

where $\bar{\lambda}$ is the reduced de Broglie wave length, l are the orbital angular momenta and T_l are the transmission coefficients [Joh75]. With a sharp cut off approximation for T_l according to

$$T_l = \begin{cases} 1 & l \leq l_{\max} \\ 0 & l > l_{\max} \end{cases} \tag{2.2}$$

one obtains

$$\sigma_R = \pi \bar{\lambda}^2 \sum_{l=0}^{l_{\max}} (2l + 1)^2 = \pi \bar{\lambda}^2 (l_{\max} + 1)^2 = \pi \bar{\lambda}^2 l_{\max}^2 , \tag{2.3}$$

where $l_{\max}$ is the highest partial wave to fuse the nuclei.

Fusion (or compound nucleus) cross-sections σ_f have been measured for a large number of target and projectile combinations. The measurements are also done for different energy regimes. It has been realized that σ_f versus the reciprocal of the bombarding energy can be divided into different energy regions. At energies only slightly above the barrier the cross-section σ_f follows the total reaction cross-section, whereas at higher energies they fall clearly below σ_R. Different models (e.g. critical distance model, statistical yrast line model, and successive critical distance model) have been proposed to explain the measured cross-sections (see [Boc89, Lee80, Lee84, Mos81]).

For collisions between not too heavy projectiles and target nuclei, $A_1 + A_2 \leq 100$, up to an energy about twice the Coulomb barrier V_B , fusion is the dominant reaction channel and exhaust some 60 - 90% of the total reaction cross-section σ_R. In the energy interval from

1.2V_B up to 2 V_B, l_{max} is limited by the Coulomb barrier V_B (R_B) and the interaction radius R_B. The total excitation energy E^* of the compound nucleus is given by

$$E^* = V_B(R_B) + \frac{\hbar^2}{2\mu R_B} l_{\max}(l_{\max} + 1) + Q = E_{C.M.} + Q \quad , \tag{2.4}$$

where μ is the reduced mass of the nuclei involved, Q is the Q-value of the reaction and E_{CM} is the incident energy in the center-of-mass system. Using Eqs.(2.3) and (2.4), the fusion cross-section is given by

$$\sigma_f = \pi R_B^2 [1 - V_B(R_B)/E_{C.M.}] \tag{2.5}$$

The parameters R_B and the potential $V(R_B)$, can be determined by fitting expression (2.5) to the data. This gives

$$R_B = r_B(A_1^{1/3} + A_2^{1/3}) \ \ with \ \ r_B = (1.4 - 1.6) fm, \tag{2.6}$$

where A_1 and A_2 are the atomic numbers of the projectile and the target nucleus, respectively.

2.3. De-excitation Processes of Highly-Excited Nuclei

The compound nucleus is formed in a time scale of 10^{-22} s and it equilibrates by 10^{-20} s. With about 60 units of angular momentum a rotational frequency of around 2 x 10^{20} Hz is obtained (which corresponds to an energy of $\hbar\omega$ = 0.75 MeV) and so equilibration takes at most a couple of rotations [Twi89].

The high excitation mode of the compound nucleus results in a subsequent evaporation of particles. The emission of charged particles like protons or α-particles is hindered by the Coulomb barrier. Therefore, particle emission is usually dominated by neutron evaporation and this commences on a time scale of 10^{-19}s by which time the nucleus will have rotated about 20 times. At this stage there is a small probability (10^{-3}), relative to particle emission, of the emission of a very high-energy ($E_\gamma \sim$ 15 MeV) dipole γ-ray from a (so-called Giant Dipole Resonance). The particle emission continues until after approximately 10^5 rotations (or ~ 10^{-15}s) when the major γ-ray emission commences. The nucleus reaches its ground state in a time scale of 10^{-9}s and it has already rotated the order of 10^{11} times, i.e. only one order of magnitude less than the number of rotations of the earth since its creation. Therefore, though the time scale for different processes appear minuscule in a terrestrial frame, they are quite large when measured relative to the rotational frequency of the nucleus [Gar85, Twi89]. The pathway from the formation of a compound nucleus to the ground state of the final nucleus is illustrated in Fig. 2.2.

An emitted neutron lowers considerably the excitation energy of the nuclear system to within its separation energy (for charged-particles binding energy plus Coulomb barrier), but to a much lesser degree the angular momentum, on the average about 1ħ unit per nucleon [Gro67a].

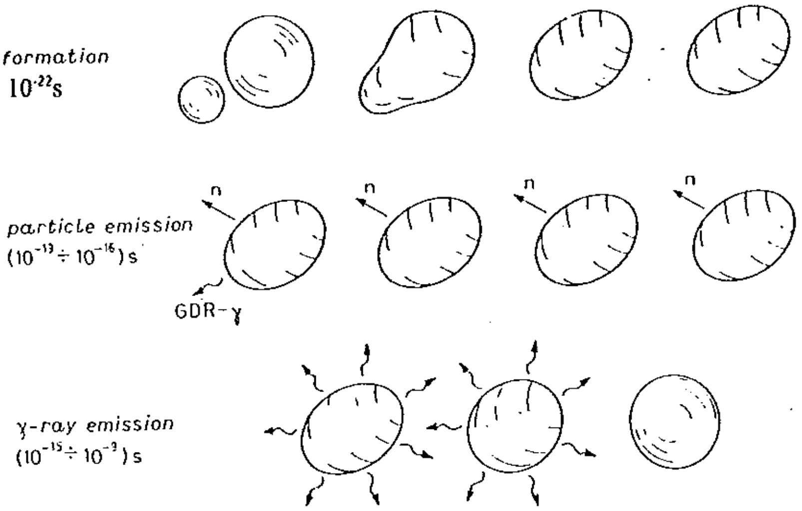

Fig. 2.2. Schematic figure depicting the formation and decay of a highly excited nucleus [Twi89].

For light nuclei, where the Coulomb barrier is lower, and for highly neutron-deficient nuclei charged-particle emission may however, compete strongly with neutron emission. The spin distribution of the compound nucleus also plays an important role. From high angular-momentum states, α-emission is favored since an α-particle can carry away more angular momentum than a neutron.

When the excitation energy in the evaporation process becomes lower than about the binding energy of one neutron above the yrast line (the line connecting the lowest states for each spin value), neutron evaporation is hindered owing to the limited amount of angular momentum the neutron preferentially carry away. On the other hand, α -particles have a larger probability to be emitted at this excitation energy. Qualitatively this is easily understood interms of two effects [Gro67b]: firstly, for equal energies and orbital angular momenta, the centrifugal barrier is a greater obstacle to the neutron than to the massive α-particle; secondly, the smallest kinetic energy at which the neutron can be emitted is zero, a " hard " absolute limit, while the lowest-energy α-particles are limited by the relative "soft" Coulomb barrier. Therefore, α-emission is believed to be a function of both the initial excitation energy and the initial angular momentum.

When not enough energy is left to emit particles, the remaining excitation energy and angular momentum is removed by the emission of γ-rays. After the initial particle evaporation, much of the area between the yrast line and the entry limit (approximately a neutron binding energy higher) is populated, and so there are a great number of pathways down to the ground state. The initial transitions have too little intensity, whereas the level densities are so large to be observed individually even with the highest resolution detectors available today, and so these transitions produce the "continuum " γ-ray spectrum. This consists of two main types of γ-rays [Gar85, Voi83]: the "statistical " one with a small number of transitions that carry off energy but little angular momentum; and the " yrast-like " transitions that run roughly parallel to the yrast line and remove the angular momentum as well as excitation energy. The " statistical " transitions " cools " the nucleus, whereas the " yrast-like " transitions have the effect of slowing down the nucleus to its ground state. Eventually, the γ-cascades lose enough energy so that they come to the region of low level density near the yrast line, and there they condenses into a small enough number of pathways, i.e., with sufficient intensity, that the individual transition can be detected, forming the discrete γ-ray spectrum. The different contributions to the γ spectrum are demonstrated with ^{152}Dy (Fig. 2.3).

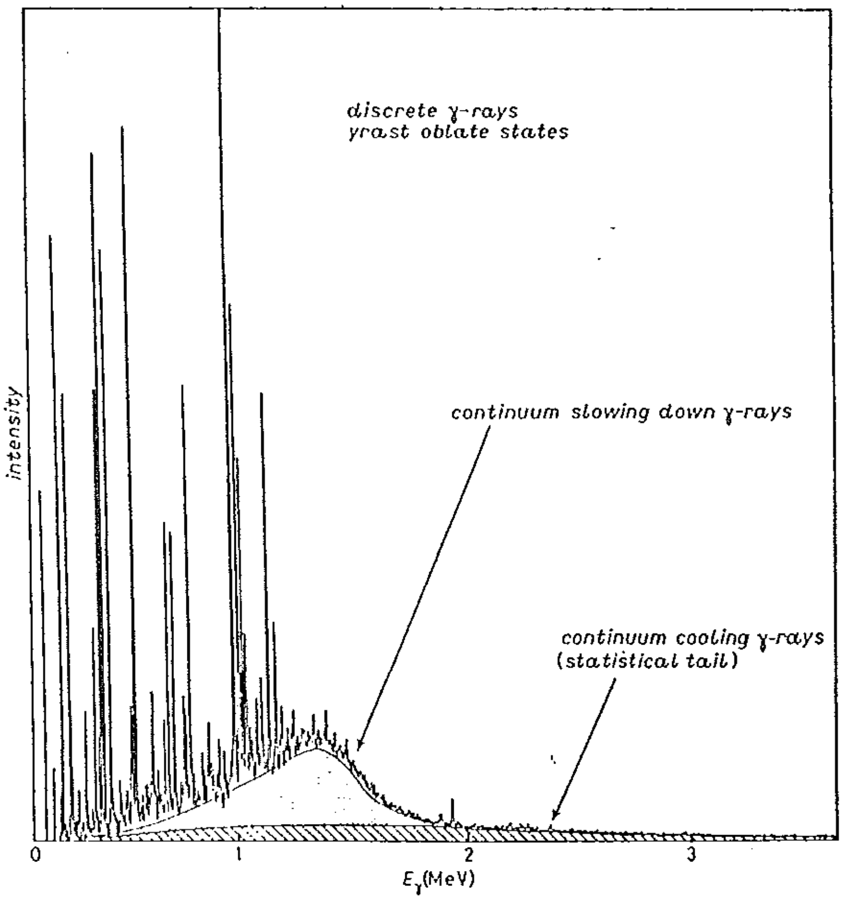

Fig. 2.3. The total γ-ray spectrum of the decay of ^{152}Dy produced in the ^{108}Pd (^{48}Ca, 4n) fusion-evaporation reaction at 205 MeV [Twi89].

To get some feeling for the relative intensities of discrete transitions, their intensities are ~ 1% at spin 40 ħ and 20-40% at spin 20 ħ in rare-earth nuclei (where the highest spin states have been observed and where much of the experimental work has been concentrated) [Dia86]. With increasingly better instruments and better statistics, one is able to push discrete γ-ray spectroscopy to larger spins (to still lower intensities).

2.4. Schematic Illustration of the De-excitation Processes

The yrast levels play a crucial role, as mentioned in sec.2.3, in the de-excitation of the excited nucleus with high angular momentum. For fixed spin I there are no levels below some lowest energy E_I ,the yrast line. The lowest energy for a given angular momentum I is given by the energy of the collective rotation

$$E_I = \frac{\hbar^2}{2\Im} I(I+1) \tag{2.7}$$

where $\Im$ denotes the total moment of inertia of the composite system. For rigid rotation of this system one obtains

$$\Im_{rig.} = \frac{2}{5} M R^2, \tag{2.8}$$

where M is the mass of the system and R is its radius. In general the moment of inertia of the nuclear system has a value [Boc89] of

$$0.5\Im_{rig.} \leq \Im \leq \Im_{rig.} \tag{2.9}$$

The emission of neutrons and the role of the yrast level are discussed in Fig. 2.4. Here, the abscissa represents the angular momentum of a nucleus I in units of h, the ordinate the excitation energy E^* (MeV).

Consider the emission of a neutron from the nucleus at the excitation energy and angular momentum at position 1. The binding energy of the neutron is represented by a vertical arrow. The canted arrow joining the vertical arrow is intended to take into account the angular momentum removed by the outgoing neutron. Now the point of the canted arrows must not fall below the yrast line, for this is the region where the residual nucleus has no levels. For the excited nucleus at position 1, however, there is still an ample region of the E^*-I plane in which the canted arrow can terminate, and thus to which neutron emission can proceed. In this case neutron emission encounters no serious restraints and proceeds with large probability. On the other hand, consider the emission of neutrons from the nucleus having the energy and angular momentum represented in the E^*-I plane of Fig.2.4 by position 2. The binding-energy arrow terminates in the forbidden region below the yrast line. The canted arrow which must terminate at or above the yrast line is thus forced to reach far to the left. Here the outgoing neutron must carry away many units of angular momentum. To do so it must penetrate an angular-momentum barrier. The neutron emission probability may thus be considerably smaller here than at position 1 [Gro67a].

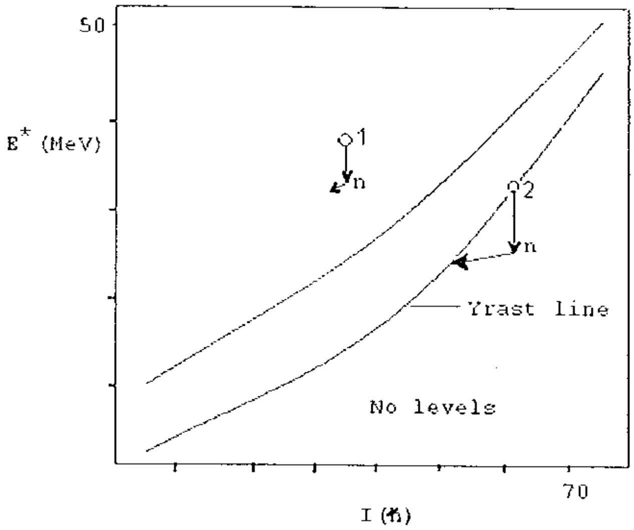

Fig. 2.4. Dependence of the excitation energy E^* Versus angular momentum I. The neutron emission property is indicated. Between the two lines the main de-excitation process is gamma-ray emission

The region enclosed between the two lines is called the " γ-cascade band " (see Fig.2.4). In the direction of the energy, the width of γ-cascade band is about one neutron binding energy, when the effect of charged particles emission can be neglected. The total de-excitation rate of an excited nucleus always includes a contribution from γ-ray emission. In this region the γ-decay is the dominant mode of de-excitation. Within this band we can distinguish two regions which make quite different contributions to the γ-spectrum. The first region is above the yrast line. This forms the continuum part of γ-emission. The second is on the yrast line itself, or very close to it, forming the discrete part of the γ-emission.

Let us now consider the de-excitation of an assembly of A^{x} nuclei, all highly excited to the same energy. They are distributed over a very wide range of angular momentum, however. The emission of a neutron (we consider only this process) from each A^{x} nucleus then gives the assembly A^{x-1} distributed over both angular momentum and energy. The emission of a second neutron similarly yields the nuclei A^{x-2} distributed over both angular momentum and energy, but the spread of energies over which most of the A^{x-2} nuclei are found is broader than it was for the distribution of nuclei A^{x-1}. Subsequent neutron emissions may broaden the energy distributions still more, of course. The feature just described is illustrated in Fig.2.5.

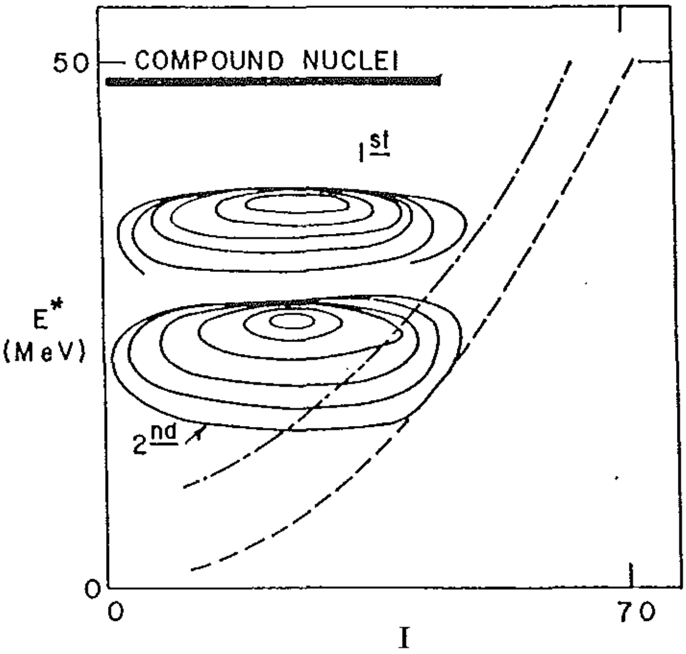

Fig. 2.5. Successive regions of energy and angular momentum populated after neutron emission (1st and 2nd regions) during the de-excitation of an assembly of highly excited nuclei [Gro67a].

The maximum energy of the A^{x-1} population distribution is less than the energy of the A^{x}. Likewise the maximum energy for any given population distribution is less than the energy of the A^{x} compound nuclei by the binding energy of the requisite number of neutrons which must be emitted to create the nucleus in question. The most probable energy for each of the successive population distribution is thus decreased by somewhat more than a neutron binding energy with each successive neutron evaporation. On the other hand, the distribution of angular momentum changes but little in the successive neutron evaporation [Gro67a]. The contour in Fig. 2.5 represents the locus of a constant relative population. The successive emission of neutrons continues until an appreciable part of the population distribution falls within the γ-cascade band. Such a situation is illustrated by the lower contour diagram in Fig. 2.5. Most of the population falling in the γ-cascade band ultimately reach the ground state via cascades of γ-ray emissions, while most of the population falling above the γ-cascade band proceed to emit another neutron.

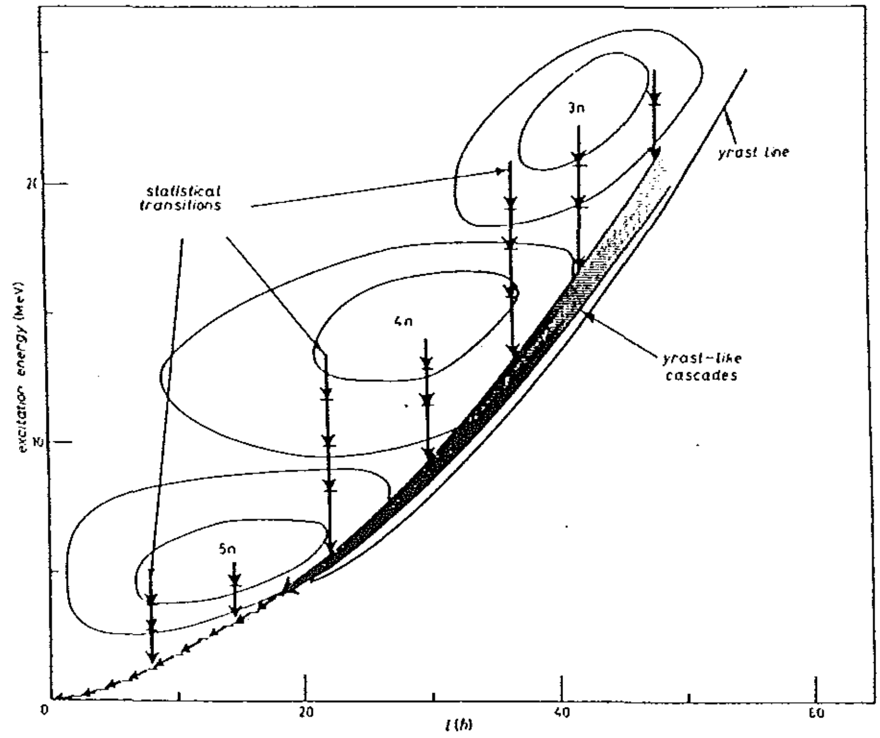

Fig. 2.6. Three phases of gamma-ray emission with the contours for 3n, 4n and 5n entry populations [Gar85].

A very popular diagram of the excitation energy versus the nuclear spin is given in Fig.2.6 [Gar85]. In the figure the different entry populations, the " statistical " transition, the "yrast-like" transition that run parallel to the yrast-line and near yrast states are clearly seen. The near yrast states are resolvable with the existing detector systems and are the basis of the present in-beam γ-ray spectroscopy.

3. Experimental and Theoretical Studies of the Mass A≈80 Region

3.1. In-Beam Gamma-Ray Spetroscopic Studies in the Mass A ≈ 80 Region

Medium and heavy nuclei display a rich variety of single-particle and collective modes of excitation. In the past nuclear structure phenomena were studied close to the ground state because of the lack of corresponding nuclear beams and multi-detector arrays to measure high excitations at a low intensity. Low-lying nuclear states are more or less compatible with shell model predictions assuming that the nucleons move independently in an average nuclear potential.

In the last decade, however, one was able to increase systematically the rotational frequency and the excitation of nuclei up to the limit of stability. It is understandable that the main interest was devoted to the rare-earth region, where many rapidly rotating nuclei have been investigated. The famous example is ^{152}Dy with a rotational band up to $I = 60\hbar$ [Twi86]. Experimental evidence that nuclei can exist as a prolate shape with ratio of the axes of 2:1 was an astonishing fact. Nuclei with mass numbers around A = 160 and 190 show sequences of γ-ray de-exciting states in superdeformed bands, which can be detected only when using arrays of gamma detectors which cover a substantial fraction of the solid angle because of the very weak populations of these states. Some of the multi-detector systems such as GAMMASPHERE , EUROGAM, GASP are already discussed in sec. 1.3.

However, a lot of questions related to nuclear structure are unsolved even in " traditional "

Table 3.1 cont'd

^{79}Sr	^{58}Ni(^{24}Mg, 2pn)	80, 85	37/2	RDM, DSAM
^{82}Sr	^{52}Cr(^{34}S, 2p2n)	130	27	GG, AD
^{83}Rb	^{82}Se(^{7}Li, α2n)	25-36	19/2	EF, GG
^{84}Sr	^{52}Cr(^{36}S, 2p2n)	130	24	GG, AD
^{85}Rb	^{82}Se(^{7}Li, 4n)	35	33/2	GG, DSA, AD
^{85}Kr	^{82}Se(^{7}Li, p3n)	32	23/2	AD, GG, PG, EF
^{86}Rb	^{82}Se(^{7}Li, 3n)	30-35	16	AD, GG, EF
^{86}Kr	^{82}Se(^{7}Li, p2n)	32	12	AD, GG, PG, EF
^{89}Nb	^{66}Zn(^{30}Si, αp2n)	123	29/2	EF, GG, AD, RDM
^{90}Ru	^{58}Ni(^{36}Ar, 2p2n)	149	16	GG, NG,PG
^{91}Mo	^{66}Zn(^{28}Si, 2pn)	120	33/2	EF, GG, AD, RDM
^{91}Ru	^{58}Ni(^{36}Ar, 2pn)	149	41/2	GG, NG, PG

*) GG - γ–γ coincidence
NG - n-γ coincidence
PG - charged particle-γ coincidence
RD - recoil distance
DSA - Doppler shift attenuation
AD - angular distribution
EF - excitation function
PT - pulsed beam lifetime

Nuclei with mass number A = 80 to 90 are of special interest, because they encompass the borderline of the transition region between deformed nuclei (near ^{76}Sr) and spherical nuclei when approaching the N = 50 shell closure. In this mass region rapid nuclear shape changes or angular momentum with particle number may occur.

The review [Lie86] focuses mainly on this mass region. It covers the neutron-deficient isotopes of Ge, As, Se, Br, Kr, Rb and Sr with proton numbers Z = 32...38. As mentioned dramatic changes of the nuclear deformation occur as function of the proton and neutron number because of the oblate-prolate shape co-existence and the alignment of $g_{9/2}$ protons and neutrons.

This interesting behaviour is demonstrated in Fig. 3.1, showing the powerful tool of creating nuclei under extreme conditions using heavy-ion collisions. Recently a new region of deformed nuclei was discovered with the N = Z nucleus ^{80}Zr in the center. Shown are the excitation energies of the first 2^+ states of N = Z even-even nuclei from ^{64}Ge to ^{84}Mo together with their corresponding deformation parameters β_2 indicating strongly deformed ^{76}Sr and ^{80}Zr nuclei with β_2 around 0.4. Obviously there is a strong correlation between largest β_2 values and small E(2^+) transitions.

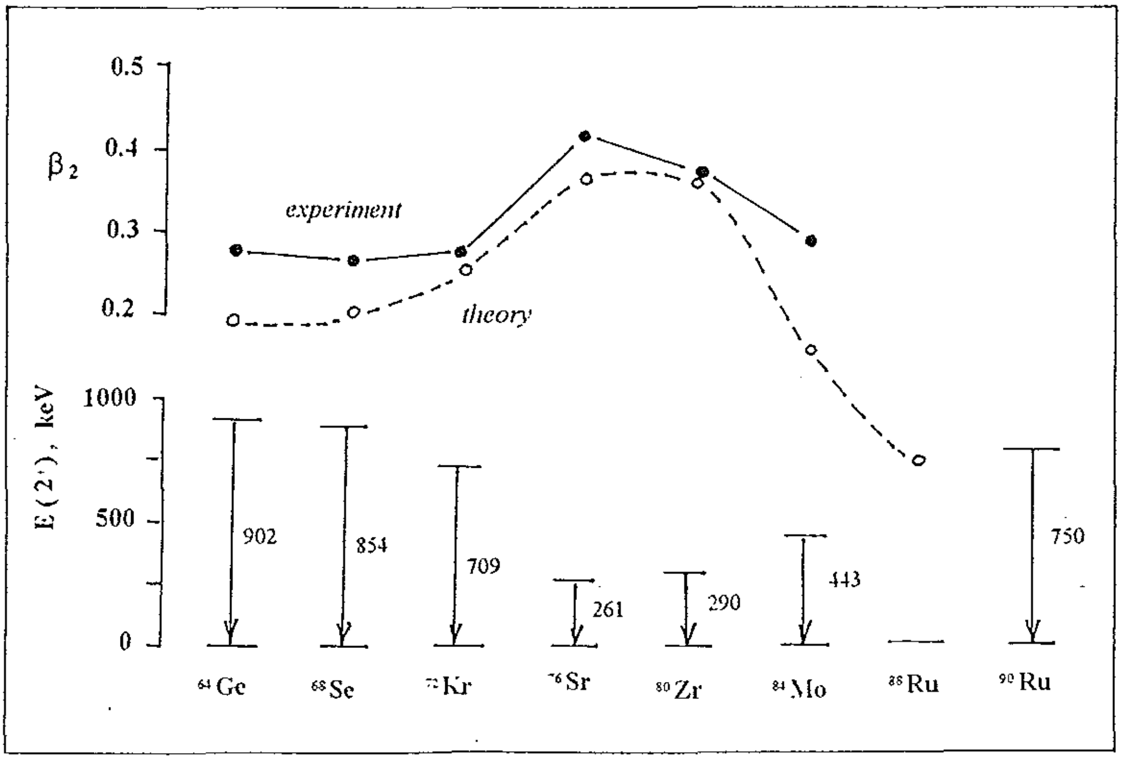

Fig. 3.1. The behaviour of theoretical and experimental values of the quadrupole deformation parameter β_2 for nuclei around A = 80 and the corresponding E(2^+) transitions.

An interesting deformation pattern is also seen in the Sr isotopes with A = 76-82. While the self-conjugate nucleus ^{76}Sr with N = Z and ^{78}Sr were found to have extreme prolate deformations with $\beta_2 = 0.38$, this value decreases to 0.29 for ^{82}Sr [EAS 87].

Recently the level scheme of the odd-odd nucleus ^{72}As [Doe94] has been investigated using the reactions ^{59}Co (^{19}F, αpn) and ^{65}Cu (^{12}C, αn) at 55 MeV and 50 MeV, respectively. From earlier work it was known that all experimental data obtained so far including the magnetic moments of ^{72}As were successfully described in terms of the nuclear shell model without any assumption of nuclear deformation. There was, so far, no need to assume any collective properties in the excited states.

However, large quadrupole deformations were found in the neighbouring neutron-deficient nuclei, for instance in the odd-odd ^{74,76}Br nuclei (see, e.g. [Doe93]). The result of the new work of Doering et al. [Doe94] is: the band properties like level spacing and enhanced E2-transitions point to a collective excitation in ^{72}As based on the two quasi-particle configuration $\pi g_{9/2} \otimes \nu g_{9/2}$. Thus, the occupation of the $g_{9/2}$ subshell was found in ^{72}As. The measured E2-strengths reveal an average quadrupole deformation of $\beta_2 \approx 0.26$ if axial symmetry is assumed. This onset of substantial deformation and collectivity in ^{72}As is somewhat unexpected in view of its low-spin behaviour (I up to 15 has been found) but is in agreement with a cranking shell model [Naz85].

The Fermi gas model [Boh69] predicts for the total level density $\rho(E)$

$$\rho\,(E) \;=\; \frac{6^{1/4}}{12}\,\frac{g_o}{(g_o E\,)^{5/4}}\,\exp\left\{2\,(\,\frac{\pi^2}{6} g_o E)^{1/2}\right\} \qquad (3.1)$$

where N ≈ Z, E is the excitation energy and g_o is the one-particle level density at the Fermi energy, representing the sum of the proton and neutron level densities,

$$g_o \equiv g(\varepsilon_F) \approx \frac{3}{2}\frac{A}{\varepsilon_F}. \tag{3.2}$$

The quantity ε_F represents the maximum kinetic energy of a particle in the Fermi gas and is given by

$$\varepsilon_F = (\hbar k_F)^2/2M \approx 37 MeV. \tag{3.3}$$

The parameter

$$a = \frac{\pi^2}{6} g_o \tag{3.4}$$

which appears in the exponent of Eq. (3.1) is the nuclear level density parameter, and can be determined, e.g. from the resonance spectra of slow neutrons, the direct count of levels populated in charged particle nuclear reactions or from the analysis of particle evaporation spectra [Boh69].

Different phenomenological approaches were developed to describe the anomalies in the A-dependence of the level density parameter. An extensive analysis of these various prediction and their comparison with the experimental findings has been carried out by Mashnik [Mas93]. There are seen several characteristic regions in the A-dependence of the parameter a, among then the mass region A = 70-90, where the level density parameter drops down dramatically from a value a $\cong$ 14 MeV^{-1} to $\cong$ 7 MeV^{-1}. This behaviour is also a strong indication for interesting nuclear structure physics of that mass region under consideration.

From the point of view of modern nuclear structure investigations the properties of high-spin states in this mass region are of special interest. As the experimental findings indicate, a rich variety of different shapes evolving with spin in the same nuclei can be determined [Bak82]. We start the discussion of mass A = 70-90 nuclei with a very recent measurement of high-spin states of ^{84}Sr [Gur94] with the Oak Ridge Compton-Suppression Spectrometer system (18 Ge- detectors and 52 elements of the Spin Spectrometer to measure gamma ray multiplicities) [Jaa83]. When using the reaction ^{52}Cr(^{36}S, 2p2n) at 130 MeV the level scheme has been extended up to I = 24 at 15084 keV excitation energy for the positive parity band. The Sr isotopes have proton number (Z = 38) and, in particular ^{84}Sr is only four neutrons away from the N = 50 closed shell. Therefore, ^{84}Sr presents a nuclear structure characteristic of a "spherical" nucleus.

Previous works of Dewald et al. [Dew82] used the reaction ^{76}Ge (^{12}C, 4n) to populate states in ^{84}Sr up to 6070 keV. They reported a maximum angular momentum of 14 $\hbar$. The new gamma cascade measured presents a regular increase in the γ-ray transition energy with level energy.

High-spin states of N = 49, 50 nuclei ^{85}Kr and ^{86}Kr have been investigated via the ^{82}Se (^{7}Li, p3n) and ^{82}Se (^{7}Li, p2n) reactions, respectively, using 32 MeV ^{7}Li ions [Win93]. In order to suppress γ-rays arising from pure neutron evaporation the measurements of angular distributions and relative excitation functions of the γ-rays as well as γ-γ coincidences have been performed in particle-γ coincidence mode. For this purpose 14 Si-detectors, in connection with six Ge-detectors, have been mounted inside the OSIRIS-CUBE at the Cologne tandem accelerator.

The level scheme of ^{85}Kr have been extended by a new sequences of high-spin states with excitation energies up to 4.8 MeV and tentative spins up to I = 23/2 that is built on top of the $17^-/2$ μs isomer at 1991.8 keV. For ^{86}Kr a new level scheme of high-spin states with excitation energies up to 7.9 Mev and tentative spins up to I = 12 ħ have been observed. In the same experiment the excited states of ^{86}Rb [Win94] have been studied in an in-beam experiment via the reaction ^{82}Se(^{7}Li, 3n)^{86}Rb, and the result shows that spins up to I = 16 ħ has been deduced. Shell-model calculations have been carried out to interpret these experimental results, and the level energies predicted are found to be in fair agreement with the experimental results.

High-spin states in neutron-deficient nuclei ^{90}Ru and ^{91}Ru have been studied [Hee94] in the 2p2n and 2pn reaction channels of ^{36}Ar + ^{58}Ni using the 149 MeV ^{36}Ar beam at VICKSI (Hahn-Meitner-Institute Berlin) and the OSIRIS array. This system consisted of 12 escape-suppressed Ge- detectors mounted at 65 and 115 degrees to the beam axis, seven NE213 neutron detectors and four ΔE silicon surface barrier detectors to gate the gamma measurements with evaporated neutrons and protons, respectively. The level scheme of ^{90}Ru and ^{91}Ru up to I =16 and I = 41/2, respectively, could be established independent of the weakness of the observed transitions.

The nucleus ^{95}Ru has one neutron outside the N = 50 shell. The high-spin structure of this nucleus has been studied [Ghu94] using the fusion-evaporation reaction ^{94}Zr (^{35}Cl, 3pn) at 140 MeV. About 40 new transitions could be found up to 43/2 and 39/2 in the positive and negative parity bands, respectively. As this mass number is already outside of our region of interest, we are not going to discuss the details of the structure of ^{95}Ru, but mention only the fact that up to moderate spin states in the level scheme agreement with spherical shell model calculations within a limited configuration space could be established. A weak coupling scheme in which a $2d_{5/2}$ neutron couples to the excited ^{94}Ru core was found to work reasonably well, because it reproduces the yrast spectrum of ^{95}Ru. Of course, to understand the high-spin structure a more rigorous approach would be necessary considering the breaking of the N = 50 neutron core.

In many cases the compound nucleus created in an heavy ion reaction de-excites via evaporation of several neutrons (see sec.2.3). Using medium-weight heavy ions to reach the mass region A = 80 we observe some specifics. For instance, the compound nucleus ^{80}Zr can be created in ^{40}Ca + ^{40}Ca collisions. In Fig. 3.2 predictions of the cascade-evaporation model [Lie86] are shown illustrating that the Z = N = 40 nucleus ^{80}Zr emits presumably

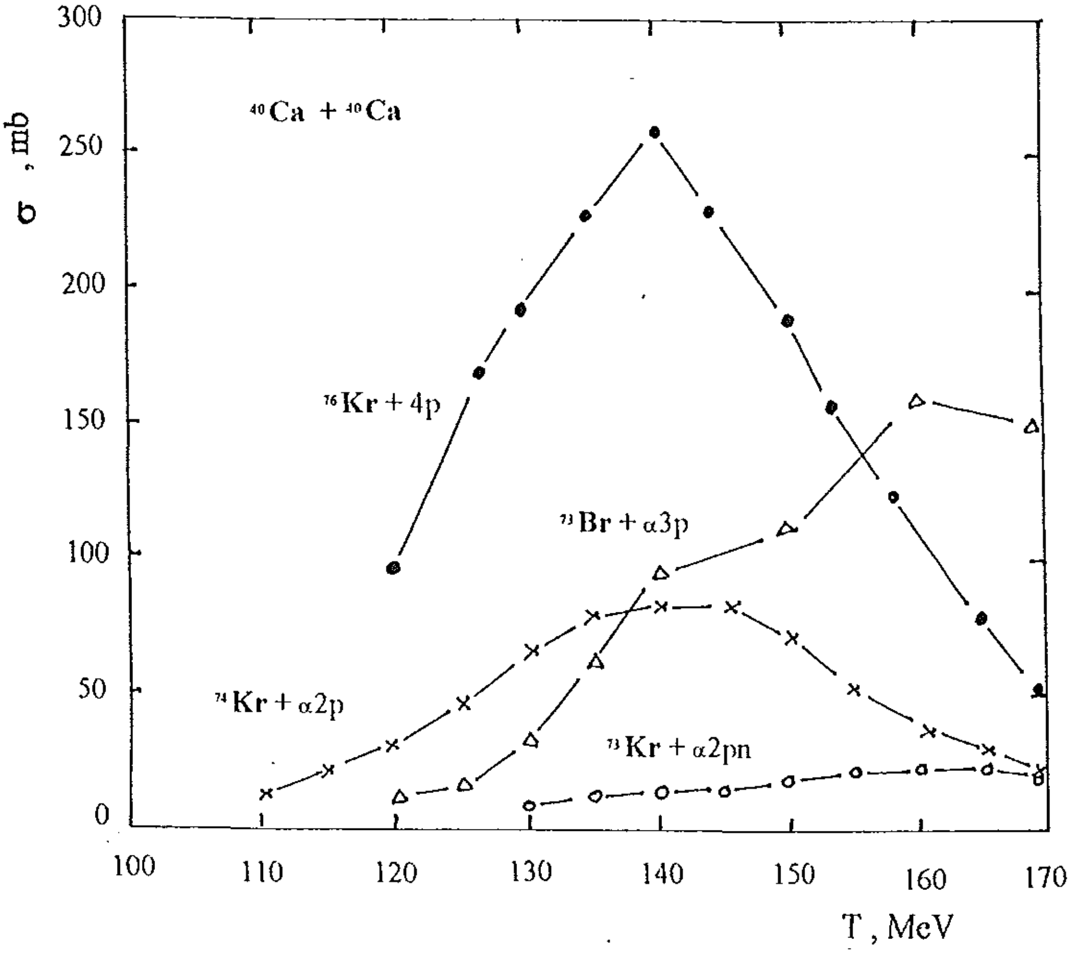

Fig. 3.2. Calculated distribution of evaporation residues in the ^{40}Ca + ^{40}Ca collisions at 110 - 170 MeV beam energy [Lie83]. Note the pre-dominant emission of protons and α-particles.

charged particles, at larger energies above 140 MeV alpha particles and protons, while the cross section for the creation of ^{73}Kr accompanied with 2pn is at least 30 times smaller than the one for the exit channel ^{76}Kr + 4p. This way neutron-deficient nuclei try " to improve " their neutron-proton ratios to larger values.

Generally a rich experimental material in the A = 70-90 region has been accumulated [Lie86] over the last decade. The nuclei involved contain Z = 32 (Ge) - 40 (Zr) protons and N = 50 neutrons. As already mentioned high-spin studies were carried out by different groups. In table 3.1 maximum values of spins identified in different reactions with light and medium heavy ions are collected. The angular momenta reached are too small that a $A \approx 80$ nucleus may undergo a transition to a superdeformed shape ($I \geq 50\hbar$) or may undergo even fission ($I \geq 75\hbar$), as predicted by liquid drop model, (see e.g. [Mol81]).

High-spin states has been studied in many nuclei of the mass region here under consideration. Interesting physics came out when comparing even-even and odd-even neighbour nuclei, e. g. shape coexistence, core polarization and pairing effects. Some of these findings compared with theoretical predictions will be discussed in sect. 3.2.

In the data analysis we will limit ourselves to the excited states of ^{85,86}Rb and ^{85,86}Kr produced in fusion-evaporation reactions of ^{7}Li with ^{82}Se at 35 MeV. These nuclei are expected to be produced with similar intensities. The ^{85,86}Rb nuclei with Z = 37 and N = 48 (49) are only two (one) neutrons and one proton away from the magic nucleus ^{88}Sr. Therefore, one can expect that collective effects of many nucleons will be of rather small influence on the excited states.

3.2. Theoretical Considerations in the Mass A $\approx$ 80 Region

Numerous experimental works were devoted to the mass region A $\approx$ 70 to 90, and the results indicate interesting nuclear structure with quick changes going from one nucleus to its neighbour. This is especially true if one moves away from the valley of β-stability. As shown in sec. 3.1, particularly neutron-deficient nuclides have been created with extreme deformations up to $\beta_2 \approx 0.4$. In this section some recent theoretical works are compared with data. One should also stress that the experimental results obtained in the mass region under consideration test rather critical the theoretical model predictions.

We start with the behaviour of collective bands and deformations in $^{76\text{-}82}$Sr nuclei. Experimentally one finds the neutron-deficient Sr isotopes to have extreme prolate deformations. The deformation decreases with filling up the neutron holes in the $g_{9/2}$ shell. An systematic study of this interesting behaviour has been carried out in [Tri94]. The authors use a deformed configuration mixing (DCM) shell model to carry out microscopic calculations. Starting with ^{56}Ni as the inert core and using 4 spherical single-particle orbits as the basic space and an effective interaction as proposed in [Aha85], the calculated positive and negative parity bands agree quite well with experiment, especially the quadrupole deformation and its variation with mass number of the Sr isotopes could be reproduced. It was shown in [Tri85] that ^{76}Sr is the most deformed nucleus in the region, in agreement with the experimental findings presented in Fig. 3.1. For ^{80,82}Sr a gradual proton alignment has been predicted.

Microscopic-macroscopic calculations have been performed for these nuclei using Yukawa [Mol84] and Woods-Saxon [Naz85] nuclear potentials. In another study the Interacting Boson Approximation (IBA) proposed by Arima and Iachello [Ari75] has been use

[Buc83]. This model provides a unified description of collective nuclear states - mainly low-energy collective degrees of freedom - in terms of a system of interacting bosons (Fermion pairs of nucleons). The IBA and its extensions has been extensively discussed, see e. g. [Fen83].

Nuclear deformations in the A ≈ 80 region were investigated also in [Gal86]. Here the Strutinsky method has been employed with which the most important progress in the description of shape transitions in this mass region has been achieved. A Nilsson-type potential and Yukawa-plus-exponential macroscopic mass formula has been selected. Special emphasis was given to the spin-orbit potential parameters, which have large variations at the magic numbers. The results obtained are similar to those of the shell model calculations with a Yukawa potential. The occurrence of large deformations in the Z = N ≈ 38 nuclei could be reproduced in the calculation. It was also found that the choice of the potential parameters is rather sensitive in this mass region A ≈ 80.

The N = 50 isotones are of particular interest to test shell model calculations. Due to the shell closure of the neutron system at least the low-lying levels can be explained by the valence protons only. However, this situation might be changed at high excitation energies with the appearance of neutron $g^{-1}_{9/2}$, $d^{-1}_{5/2}$ excitations. Such a search for core excitations has been carried out [Win93] where the high-spin structure of ^{86}Kr was investigated. Using a certain model space of active proton and neutron orbitals relative to the hypothetical ^{68}Ni core with closed proton (Z = 28) and neutron (N = 40) shells it was shown that the level energies of positive-parity yrast states with large spin up to 10 ħ are shifted towards the experiment if particle-hole excitations of the neutron core are considered.

More attention to the neutron-proton interaction must be paid in the doubly-odd nucleus ^{86}Rb containing 37 protons and 49 neutrons. The levels near the ground state are dominated by the proton (π) - neutron (ν) configuration $\pi f^{-1}_{5/2} \otimes \nu g^{-1}_{9/2}$. However, at higher spin values additional configurations must be included [Win94].

We remark finally that from the level sequences in ^{83}Br one could conclude [Sch93] that the measured transition strengths E2 and M1 point to rather non-collective configurations. This behaviour can be expected also if we fill up the proton shell to approach the Z = 50 closed shell. Indeed, for the neutron-deficient nuclei ^{90,91}Ru it has been demonstrated that the experimental level schemes can be interpreted satisfactorily with shell model calculations performed within the restricted ($g_{9/2}$, $p_{1/2}$) model space.

We notice a broad spectrum of different theoretical procedures within a limited region of the mass number. And it is not astonishing that experimental and theoretical investigations are continuing in this field around A = 80.

4. Data Acquisition and Data Analysis

4.1. Origin of the Data and Experimental Set Up

The data were taken at the cyclotron of the Forschungszentrum Rossendorf in Germany. During the experiment a self-supporting target of ^{82}Se, enriched to 92%, of thickness 8mg/cm^2 was bombarded by ^{7}Li ions at beam energy of 35 MeV. The detector used during the experiment was an intrinsic Ge-detector with 10% relative efficiency. The position of the Ge-detector was 90° relative to the beam direction (Fig. 4.1)

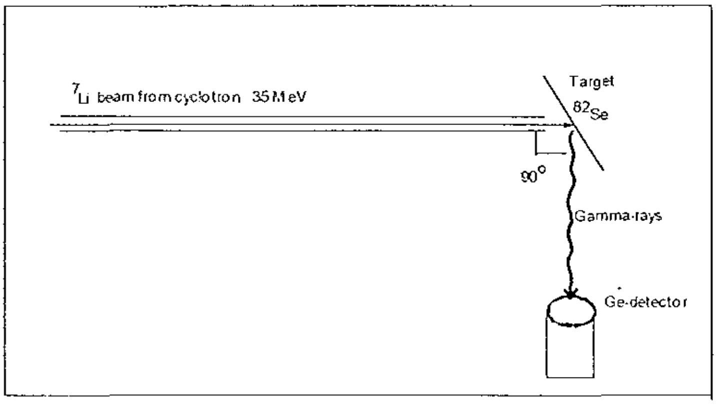

Fig 4.1 Schematic of the experimental set up

The fact that heavy-ion fusion-evaporation reactions are not selective in the production of the final nucleus of interest makes the γ-ray singles spectrum rather complicated. Several competing reactions contribute to the singles spectrum (sec. 4.2.3). The result of an in-beam measurement for the reaction ^{7}Li incident on ^{82}Se is shown in Fig. 4.2.

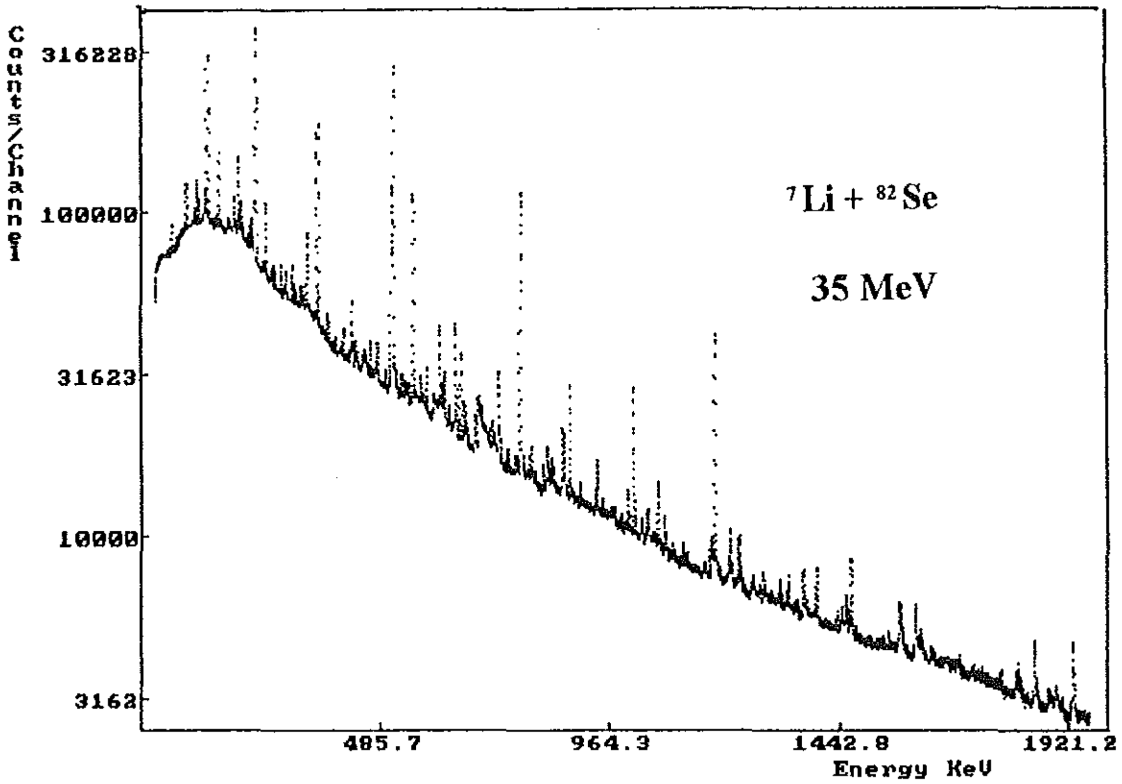

Fig. 4.2. Gamma-ray singles spectrum of the reaction ^{7}Li + ^{82}Se measured at 90° relative to the beam direction.

From Fig. 4.2 one can see that the line spacing is small at lower energies and increases at larger γ-energies. To show this behaviour of the spectrum, the number of transitions versus channel number is given in Fig. 4.3. This transition distribution could be fitted by an exponentially decaying function.

This experimental finding can not be directly compared with theoretical considerations e.g. in the Fermi gas model, because the transitions are summed up from different final nuclei produced. Nevertheless, the experimental behaviour shown in Fig. 4.3 is reminiscent, for instance, to the level spacings of neutron resonances, which can be described by an exponentially decaying curve (for details see [Boh69]). This behaviour points to the fact

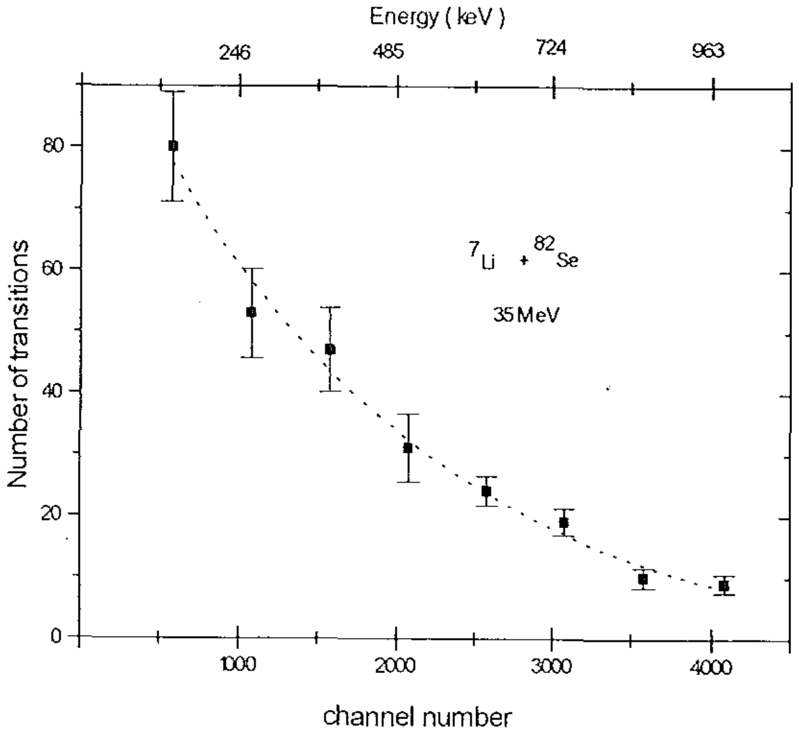

Fig. 4.3. Distribution of transitions in the spectrum versus channel number. The upper abscissa gives the corresponding energy intervals of the transitions.

that the de-excitation of the compound nuclei produced is a statistical process, i.e. it comes from the exponential increase of the level density with excitation energy [Daw63].

In the singles spectrum almost 270 transitions could be seen in an energy interval between 46 and 1931 keV. Among them are also the ^{60}Co-lines (see App.A table A2, channel Nos. 4876.36 and 5540.78) arising from activation of beam lines and construction materials. To demonstrate how complicated the spectrum analysis is, a spectrum obtained from neutron activation is shown for the same energy range in Fig.4.4 (this spectrum was provided by the IAEA together with the GANAAS package).

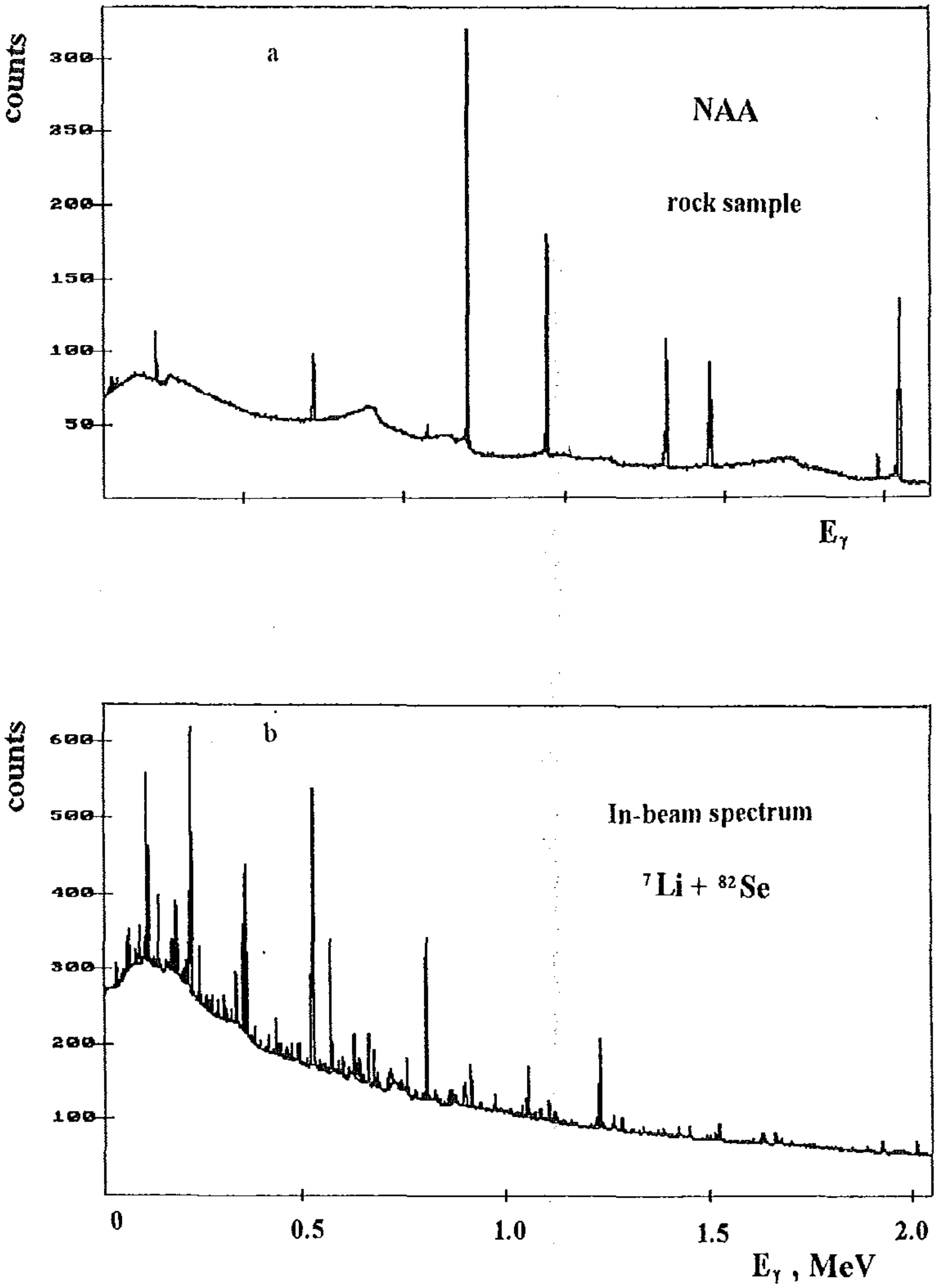

Fig. 4.4. Comparison of the spectra obtained in neutron activation of a rock sample (a) and from in-beam measurement of the reaction ^{7}Li + ^{82}Se (b). The number of transitions measured in the in-beam experiment is 10 times larger than that of the NAA spectrum.

The complexity of singles spectrum from an in-beam measurement is even larger when the detector position relative to the beam direction is different from 90°. In this case as a result of the Doppler effect additional lines or at least a line broadening appear in the singles spectrum thereby increasing the complexity. This effect is demonstrated in Fig. 4.5 where at 35° an additional line appears from the Doppler effect of the 1017 keV-line.

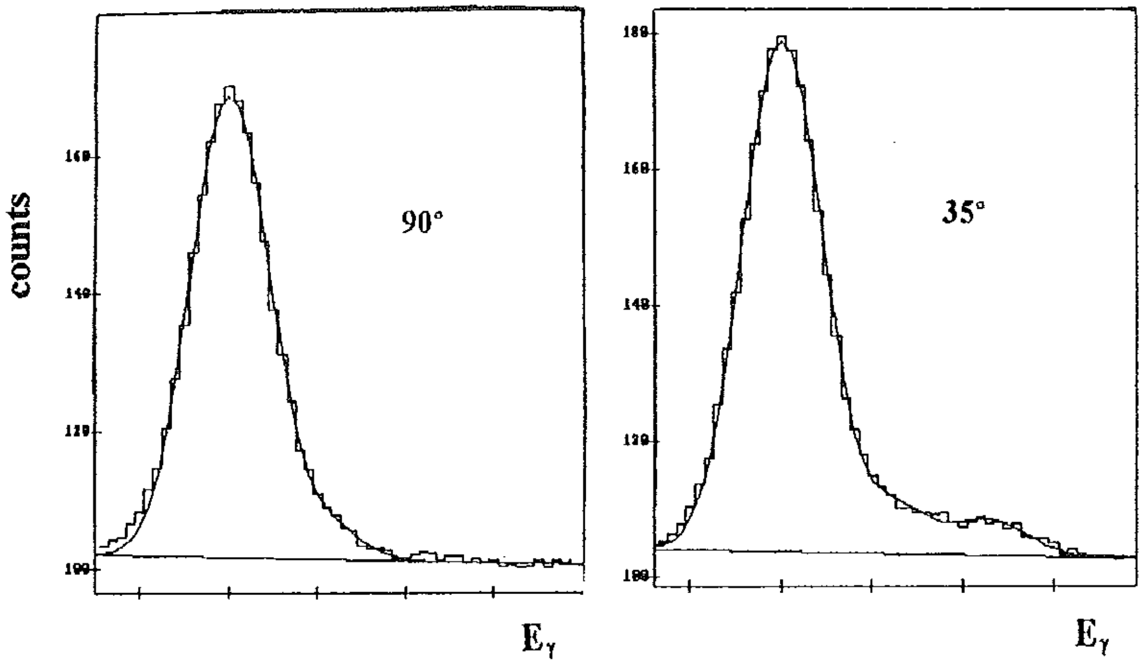

Fig. 4.5. Demonstration of the Doppler effect. In the 90° spectrum an isolated line at 1017 keV is found, whereas in the 35° spectrum an additional line (shifted by ~ 3 keV) due to the Doppler effect appears.

Therefore, we selected for the data analysis a spectrum measured at 90°, where the Doppler effect is at minimum.

4.2. Data Analysis

The data we are considering is a singles spectrum from an in-beam measurement of the reaction ^{7}Li incident on ^{82}Se. We simply limit our analysis to the nuclei $^{85\text{-}86}$Kr and $^{85\text{-}86}$Rb. High spin states of these nuclei have been investigated with the help of modern detector arrays.

Excited states of ^{85}Kr and ^{86}Kr have been investigated in the ^{82}Se (^{7}Li, p3n) and ^{82}Se (^{7}Li, p2n) reactions, using a 32 MeV ^{7}Li beam from the cyclotron in Rossendorf and the FN-tandem accelerator in Cologne. With a detector array of Ge-and Si-detectors particle-γ coincidence measurements were done to identify these nuclei [Win93]. High-spin states in ^{85}Kr are found to extend up to 23/2 ħ and those of ^{86}Kr up to 12 ħ.

The interpretation of the level schemes has been carried out within the shell model. For ^{86}Kr it is quite remarkable that the inclusion of neutron-core excitations (^{86}Kr contains N = 50 neutrons, i.e. the ground state is characterized by a closed $1g_{9/2}$ neutron shell) results in an improved agreement between experimental and calculated level energies. In the same experiment the excited states in ^{85,86}Rb were also investigated with the ^{82}Se (^{7}Li, 4n) and ^{82}Se (^{7}Li, 3n) reactions, respectively. For ^{85}Rb spins up to 33/2 ħ [Win89] and for ^{86}Rb up to 16 ħ have been deduced.

We concentrate our analysis to these nuclei and try to get the energies and intensities of the transitions accessible with a singles spectrum and compare the result with published ones. To do this we use the nuclear analysis software GANAAS (Gamma Spectrum Analysis, Activity Calculations and Neutron Activation Analysis).

4.2.1. Description of the Software Package GANAAS

GANAAS is one of the software packages developed under the auspices of the International Atomic Energy Agency (IAEA). It consists of several programs [Man91], the main modules being *the main installation module, the parameters set up, the analysis program, the activity analysis program and the concentration determination program, as well as additional utilities as gamma-ray library, and spectrum transfer and reformatting procedures*. The duties of each subprogram is described as follows.

Before starting data analysis, a number of parameters must be defined. These include calibration data (Energy, FHHM, and Efficiency calibrations), instruction of how to run the program and identification tags. These are included in the *parameters set up* subroutine. This results in an input file (*.PAR) which specifies all the parameters required for the analysis of a spectrum. Completing all the preparation for spectral analysis (parameters set up) one can go to the *analysis program*. This permits the selection of the appropriate input file, and the spectra to be analyzed, performs the γ-ray spectrum analysis, and displays the results. The results of the analysis are stored in a file with extension *.GSR. The visual inspection can be made by using a temporary file with the extension *.GGR, this file only exists for the last analyzed spectrum. The results of the analysis gives the fitted spectrum and a table containing channel number, peak energy (keV), FWHM (keV), peak area (counts) and the reduced-quality of fit χ^2 (see table A2).

After proper set up and calibration of a spectrum the activities of unknown sample can be determined. This part in GANAAS is carried out by the *activity analysis* routine. *Activity* *analysis* results in a report on the activity content of the measured sample. The results are collected in the file with the extension *.ACR.

The calculation of concentrations in GANAAS is done with the routine *concentration determination*, and is intended for Neutron Activation Analysis (NAA) work. This proceeds in two stages. First, the concentration of elements is calculated using the peak areas from the spectrum result (*.GSR) file. In the second stage, a suitable calibration standard source can be used, if available, and based on the known concentration in this standard source the correction factors for each element can be introduced. The results are stored in a file with extension *.NAR.

The program GANAAS has two library manager routines (nuclides and NAA library managers) included in the *utilities* module. The nuclide library manager is intended in particular for those users who are interested in the determination of radioactivity of their samples. This applies to the low-level counting measurements of natural or man-made radioactivity, as well as to studies related to fundamental nuclear structure research. The NAA library manager is very specifically intended for the calculation of concentration of elements in the samples irradiated by neutrons. Every user can also create his own library, corresponding to his samples, and the elements contained therein.

GANAAS must have also *Spectrum reformatting* and *transfer* programs because data can be taken with different multichannel analyzer (MCA) boards. Reformatting the spectra recorded by different multichannel analyzers to the format required for input to the GANAAS analysis program is managed by the *spectrum reformatting* program. The GANAAS input spectra have the extension *.SPE. This enables the use of many different

MCA systems (Canberra, Nucleus, Ortec etc.) as the data acquisition devices serving GANAAS. To perform the spectrum analysis, the file with the spectrum, in the suitable format, should be available and accessible to the analysis program. For a stand-alone multichannel analyzer, the spectra have to be transferred to the computer. For this a transfer program is required. For some MCA's (Canberra and Ortec series) Such transfer software is available in GANAAS.

The structure and organization of the software package GANAAS, and the extensions of files used in different GANAAS modules is shown in Fig. 4.5.

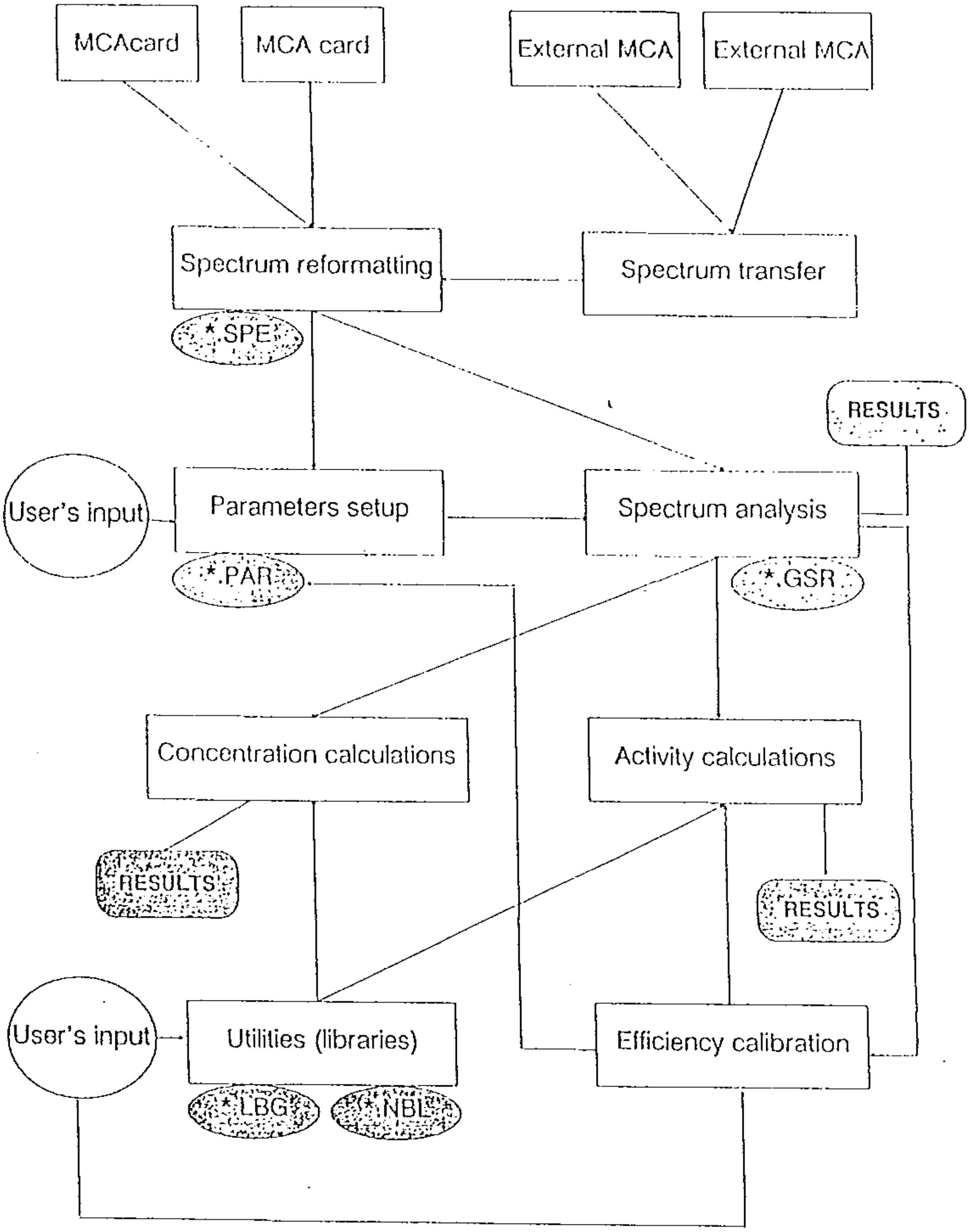

Fig. 4.5. The different programs and organization of the software package GANAAS.

4.2.2. Energy and Full Width Half Maximum (FWHM) Calibrations

The determination of the γ-ray energies and their intensities are vital for the data analysis. Every gamma spectrometer must be calibrated with special standard sources. This calibration must then be included in the software package used for the analysis. Separate calibration γ-ray sources are conventionally used to supply peaks of known energies in the spectrum, and γ-ray energies that are not widely different from those to be measured in the unknown spectrum are needed for accurate calibration. Because even the best spectrometer systems often show weak nonlinearities (one or two channels over a full range of several thousand channels), it is useful to have multiple calibration peaks at various energies along the measured energy range to account for those nonlinearities.

In our case we obtained the energy calibration from the group who has done the experiment. The equation we received has the linear dependence between the energy of the γ-ray in keV and the channel number according to

$$E_\gamma = 6.948 + 0.239256 * channel \; . \qquad (4.1)$$

What we have to do is to restore the same equation by selecting peaks from the spectrum to be analyzed. For this purpose the GANAAS program has the facility to select peaks and enter the corresponding energies (see [Man91]). The energies for each peak selected for calibration are obtained using Eq. 4.1. Once the peak selection and entering the corresponding energies is over GANAAS will display the energy calibration equation and the relation between energy versus channel number (table or graph).

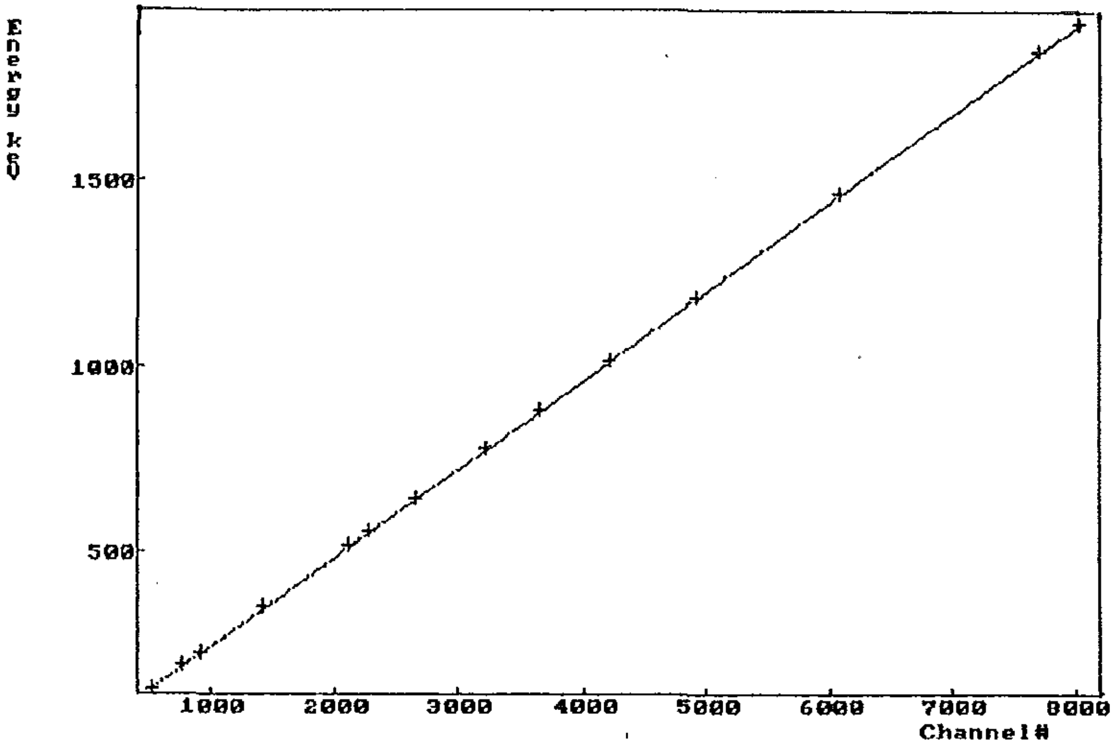

Fig. 4.6. Energy calibration for the singles spectrum obtained from in-beam measurement via the reaction ^{7}Li + ^{82}Se.

To restore Eq. 4.1 we have selected thirteen peaks (see App.A table A1) and the straight-line dependence

$$E_\gamma = 6.955 + 0.2394 * channel \tag{4.2}$$

between the energy and channel number is obtained (Fig. 4.6).

The program GANAAS must also have facility to obtain the correct energy-dependent FWHM calibration of the lines. The calibration procedure is similar to that of the energy calibration. After the peak selection and inputting the corresponding energies GANAAS displays the FWHM calibration coefficients and the curve $(FWHM)^2$ versus γ-ray energy.

The FWHM calibration requires great care. The peaks selected should be well defined singlets, with good statistics. To decide if a particular peak can be used for the calibration one can expand the peak and inspect if its shape is suitable for calibration. Selecting peaks that do not satisfy this condition will result, in general, in a nonlinear dependence between the square of the FWHM and energy. As a result one will get irrelevant fitted data with unusually large χ^2 (reduced-quality of fit) values.

Our spectrum is very complicated and practically no well defined singlets could be found. Therefore, we could not choose the FWHM calibration peaks from this spectrum. Therefore, we used a spectrum included in GANAAS software package (under the file name EXAMPLE.PAR) for demonstration purposes. This spectrum was obtained using a Ge-detector similar to the one used in the in-beam experiment. Therefore, the FWHM of peaks in this spectrum is similar to the peaks in our spectrum. This spectrum has well defined singlets peaks with good statistics. Hence, it is justifiable to use this spectrum for our FWHM calibration.

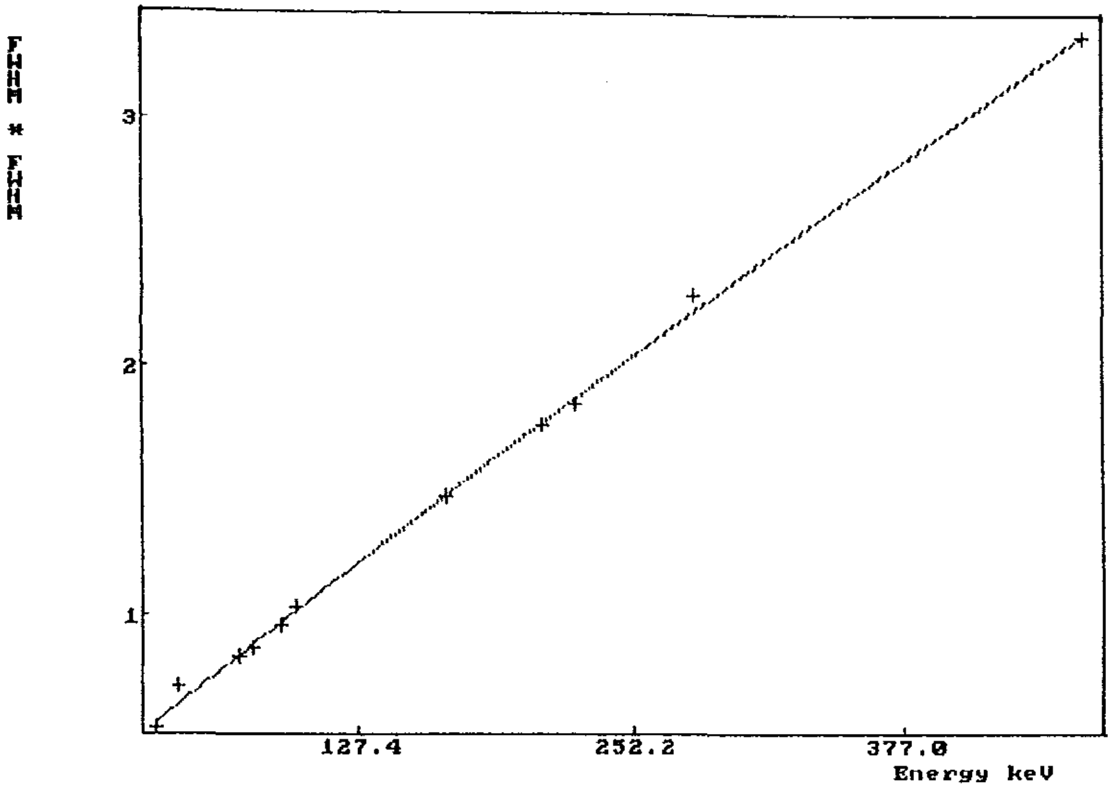

Fig. 4.7. The square of the FWHM of the lines in dependence on the γ-energy.

We have selected eleven peaks (see [Man91]) for the FWHM calibration, and the dependence between FWHM and energy we obtained was

$$\text{FWHM} = 0.2984 + 0.001841{*}E_\gamma \text{ (in keV).} \tag{4.3}$$

Once the spectrum under investigation is calibrated analysis is possible. Part of the singles spectrum fitted with GANAAS is shown in Fig. 4.8.

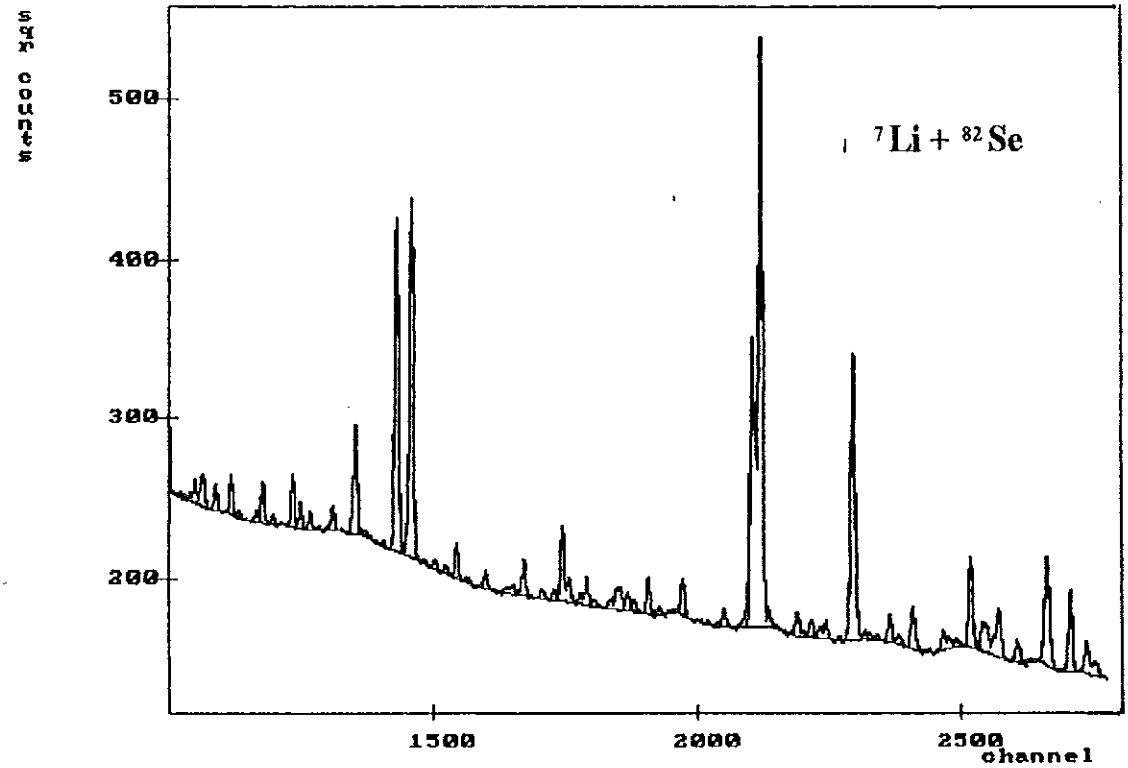

Fig. 4.8. Part of the spectrum (~ 430 keV to ~ 650 keV)fitted with GANAAS. The fitted background (the line below the peaks) is also shown.

4.2.3. Decomposition of the Spectrum

For a given entrance channel of a compound nuclear reaction there are a number of final nuclei produced as a result of different particle emission from the compound nucleus. In the reaction ^{7}Li + ^{82}Se the possible final nuclei are isotopes of Rb, Kr, Br, and Se (table 4.1).

Table 4.1. Possible reactions when ^{7}Li is incident on ^{82}Se and the corresponding Q-values.

Isotope	Possible reaction	Q-value (MeV)
${}^{85-88}_{37}Rb$	^{82}Se (^{7}Li , 4n) ^{85}Rb	-12.8
	^{82}Se (^{7}Li , 3n) ^{86}Rb	-4.2
	^{82}Se (^{7}Li , 2n) ^{87}Rb	5.76
	^{82}Se (^{7}Li , n) ^{88}Rb	11.84
${}^{85-88}_{36}K$	^{82}Se (^{7}Li , p3n) ^{85}Kr	-12.7
	^{82}Se (^{7}Li , p2n [t]) ^{86}Kr	-2.86 [5.62]
	^{82}Se (^{7}Li , pn) ^{87}Kr	2.66
	^{82}Se (^{7}Li , p) ^{88}Kr	9.71
${}^{83-87}_{35}B$	^{82}Se (^{7}Li, 2n [^{6}He, 2p4n]) ^{83}Br	-2.25 [-1.3, -30.54]
	^{82}Se (^{7}Li, n [^{5}He, 2p3n] ^{84}Br	4.6 [3.7, -23.7]
	^{82}Se (^{7}Li, 2p2n [α]) ^{85}Br	-14.8 [13.5]
	^{82}Se (^{7}Li, 2pn [^{3}He]) ^{86}Br	-9.7 [-1.98]
	^{82}Se (^{7}Li, 2p) ^{87}Br	-3.41
${}^{83-86}_{34}Se$	^{82}Se (^{7}Li , 3p3n [^{6}Li , αd]) ^{83}Se	-33.43 [-1.44, -2.91]
	^{82}Se (^{7}Li , 3p2n [αp]) ^{84}Se	-24.75 [3.55]
	^{82}Se (^{7}Li , 3pn) ^{85}Se	-20.21
	^{82}Se (^{7}Li , 3p) ^{85}Se	-14.02

The following tables give the relative intensities and energies of the lines, emitted from different final nuclei, obtained in the GANAAS fitting procedure, compared with published data.

Table 4.2. Comparison of energies and relative intensities in the level scheme of ^{85}Rb obtained in [Win89] and in the GANAAS fitting procedure.

Ref.[Win89] Energy (keV)	Intensity	GANAAS fit Energy (keV)	Intensity	Quality of fit (χ^2)
107.2	2.7	107.5	8.6	6
192.6	7.7	192.7	18.9	77
228.1	18	228.3	43.4	2
349.9	27	350.0	43.2	1
436.1	2.7	436.2	2.6	1
514.0	100	514.2	100	6
622.1	6.1	622.2	4.4	6
644.3	15	644.4	10.3	1
662.3	2.6			
662.6	0.6	662.5	2.9	5
662.6	1.0			
724.1	2.9	724.1	1	1
771.2	1.8	771.4	0.9	2
779.3	86	779.4	46.7	9
1014.3	21	1014.6	9.6	2
1176.6	2.7	1177.1	1.4	1
1183.3	57	1183.6	18.2	5
1283.9	2.6	1284.4	0.7	1
1365.8	2.3	1366.3	1.2	1
1392.6	2.9	1392.7	1.3	1
1820.7	1.1	1820.7	0.2	1

Table 4.3. Comparison of energies and relative intensities in the level scheme of ^{86}Rb obtained in [Win94] and in the GANAAS fitting procedure.

Ref.[Win94] Energy (keV)	Intensity	GANAAS fit Energy (keV)	Intensity	Quality of fit (χ^2)
125.2	62	125.4	53	1
129.9	34	130.2	38	25
144.4	2.6	144.4	3.3	1
224.3	100	224.4	100	5
263.8	4[c]	263.7	4.9	11
287.7	1.4	287.9	1.6	1
331.5	28[c]	331.7	16	6
447.0	1.4	446.8	< 1	4
556.2	5.6[c]	—	—	—
685.9	2.3	—	—	—
732.8	42	733.1	10	5
778.1	63	779.4	64	9
865.4	17	866.1	5.4	7
903.6	6.5	904.0	1.4	1
957.3	1.5[c]	—	—	—
973.7	8.5[c]	974.0	< 1	1
995.4	2.5[c]	—	—	—
1002.4	12	1002.8	2	1
1161.8	4.9	—	—	—
1427.5	0.5[c]	—	—	—
1453.7	6.5[c]	—	—	—
1598.2	19	1598.5	1.6	1
1738.7	2.8[c]	—	—	—
1814.1	3.6[c]	—	—	—
1881.7	5.7[c]	1881.7	3.2	1
1894.7	1.2[c]	—	—	—

c) Obtained in coincidence measurements

Table 4.4. Comparison of energies and relative intensities in the level scheme of ^{85}Kr obtained in [Win93] and in the GANAAS fitting procedure

Ref.[Win93]		GANAAS fit		quality of fit
Energy (kev)	Intensity	Energy (keV)	Intensity	(χ^2)
60.2	12	60.3	59	1
269.0	24	269.1	193.1	1
307.0	27	307.0	202.7	4
319.9	2	319.5	37.3	1
342.4	≈1	—	—	—
679.2	8	—	—	—
1075.8	2	—	—	—
1261.3	≈2	1261.0	25.5	1
1543.6	26	1543.9	19.2	1
1611.6	23	1261.0	18.7	1
1812.6	13	—	—	—
1931.6	100	1931.4	100	1

Table 4.5. Comparison of energies and relative intensities in the level scheme of ^{86}Kr obtained in [Win93] and in the GANAAS fitting procedure.

Ref.[Win93] Energy (keV)	Intensity	GANAAS fit Energy (keV)	Intensity	Quality of fit (χ^2)
154.2	16	154.3	87	4
247.8	13	248.1	62	1
262.8	15.5	263.7	155.1	11
325.3	4	—	—	—
416.9	11	416.0	43.3	3
433.5	20	433.4	41.5	1
495.5	7.5	—	—	—
614.2	18	614.6	109.7	6
629.3	9.5	629.9	44.7	1
685.3	100	685.7	100	1
691.6	20	692.8	193.6	27
758.2	≈ 4	—	—	—
880.0	≈ 5	—	—	—
904.4	5	904.0	43.8	1
967.0	8	967.6	7.8	1
1058.7	10	—	—	—
1211.5	≈ 4	—	—	—
1238.6	5	—	—	—
1313.7	3.5	—	—	—
1391.8	4	—	—	—
1564.8	110	1565.1	47.9	1
1566.3	35	—	—	—
1596.2	7	—	—	—
1685.1	12.5	—	—	—
1814.1	34	1813.6	21.4	1

4.2.4. Results of Data Analysis and Discussion

In this section the results of the GANAAS fit of the singles spectrum measured at 90° from the ^{7}Li + ^{82}Se reaction are discussed. As it can be seen from tables 4.2 to 4.5 for ^{85,86}Rb and ^{85,86}Kr, in all these nuclei the gamma energies fitted by GANAAS are in good agreement with published data of refs. [Win89,Win93, Win94].

In general the relative intensities obtained from the GANAAS fits are found to be larger for lines at lower energies and lower at higher γ-energies when compared to the corresponding values of refs.. [Win89, Win93, Win94] (see tables 4.2 to 4.5). The reasons for this behaviour are as follow.

One reason for this is related to the response function (efficiency) of the Ge-detector used. A typical efficiency curve for a Ge-detector is shown in Fig.4.9. It shows that at lower energies the efficiency is high and as the energy increases the efficiency goes on decreasing. Therefore, if one corrects the data for the response function of the detector (by dividing the intensities by the corresponding efficiency) the intensities at lower energies will be reduced

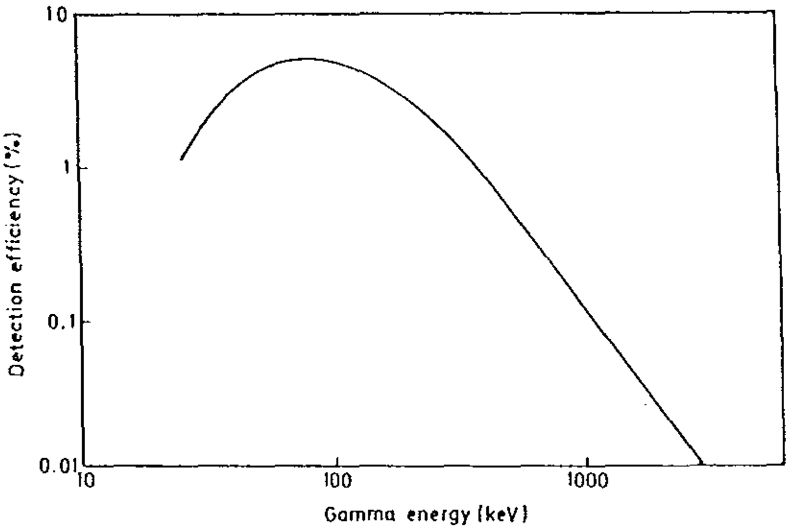

Fig. 4.9. Typical efficiency curve for a Ge(Li) detector, plotted on a double-log scale [Fai81].

while those at higher energies will be increased. As a result the relative intensities from GANAAS fit will come closer to the corresponding values obtained from the refs. [Win89, Win93, Win94].

The other reason for the behaviour of the observed relative intensities at lower energies is related to the special character of the singles spectrum. At lower energies the spectrum is so densely populated with lines that no isolated peaks could be seen and hence many lines may be hidden in one peak. Therefore larger intensity are observed for the peaks in this region. The large χ^2 for these lines is a clear indication of this behaviour. Another possible source for the deviation which is applicable for any of the lines is the parameter set used for analysis. For instance, the peak search sensitivity factor is one of the parameters which may affect the intensities of the lines (see [Man91]).

More important is that the relative intensities of the lines obtained from the GANAAS fit are found to have a similar or equal pattern as those of published data. This is an important finding as the relative intensities of the γ-lines are an essential parameter to characterize the level scheme. This behaviour will be discussed for some selected nuclei accessible in the reaction ^{7}Li + ^{82}Se at 35 MeV.

A. The Nuclei ^{85,86}Rb

Excited states in the nuclei ^{85,86}Rb have been studied via the ^{82}Se (^{7}Li, 4n) and ^{82}Se(^{7}Li,3n) reactions [Win89, Win94]. For the nuclei ^{85,86}Rb excited states up to 7.1 and 7.9 MeV, respectively, have been observed.

As can be seen from table 4.2 almost all lines from ^{85}Rb could be seen by GANAAS in the singles spectrum. Even the 1820.7 keV line with very low intensity could be found because of the fact that there are no overlapping peaks near this line. The only difficulty faced by GANAAS is to resolve the three lines around the 662.5 keV line, where two of them have the same energy (see table 4.2). Instead of three lines GANAAS could fit only a single line with fit quality of 5. This peak is shown in Fig. 4.10. The longer tail of the line on the low-energy side and the residuals indicate that the line is more complex. The energies 662.3 and 662.6 keV can be resolved only in coincidence mode, and the two 662.6 keV transitions can be put into the level scheme only when using different gates in the measurement.

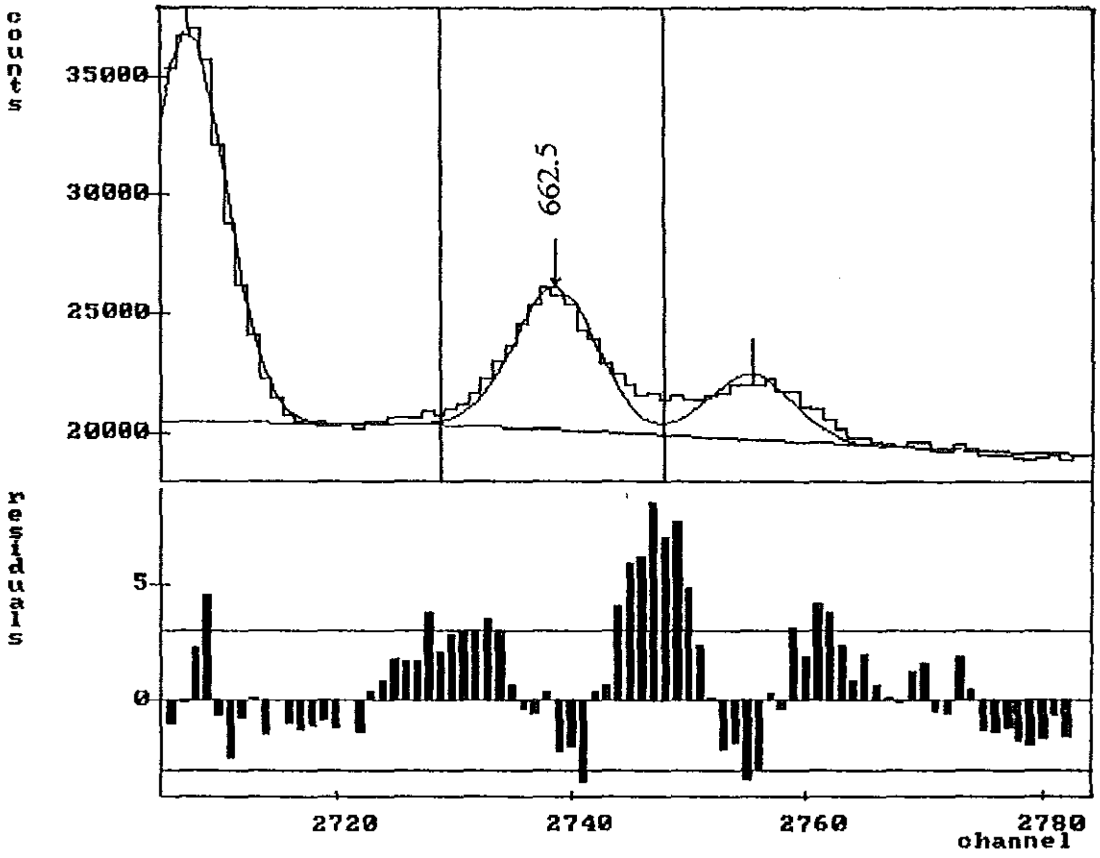

Fig. 4.10. The complex 662.5 keV peak and the corresponding residuals.

As we can see from table 4.3 of the ^{86}Rb lines and the decay scheme [Win94] (see Fig. 4.12) the main γ-cascade up to at least I = 12^+ could be identified. Difficulties arise if we go to higher spin values (low intensities), or to the side-bands or if the γ-lines were identified in the γ-γ coincidence mode. Nevertheless, the intensive lines from the side-band with γ-energies of 1598.2 and 1002.4 keV could be identified in the spectrum, even if the corresponding intensities are smaller by a factor of 12 and 6, respectively. Clearly most of the γ-transitions observed in coincidence experiments can not be seen in our singles spectrum.

As an example, we consider the 556.2 keV line of ^{86}Rb observed with an intensity of 5.6 in coincidence mode. Around this energy a peak is identified by GANAAS consisting of 3 lines at 554.4, 555.9 and 557.8 keV (see Fig. 4.11). Therefore, to isolate these lines one has to do coincidence experiments. On the other hand, the fit result demonstrates the sensitivity of the GANAAS fitting procedure.

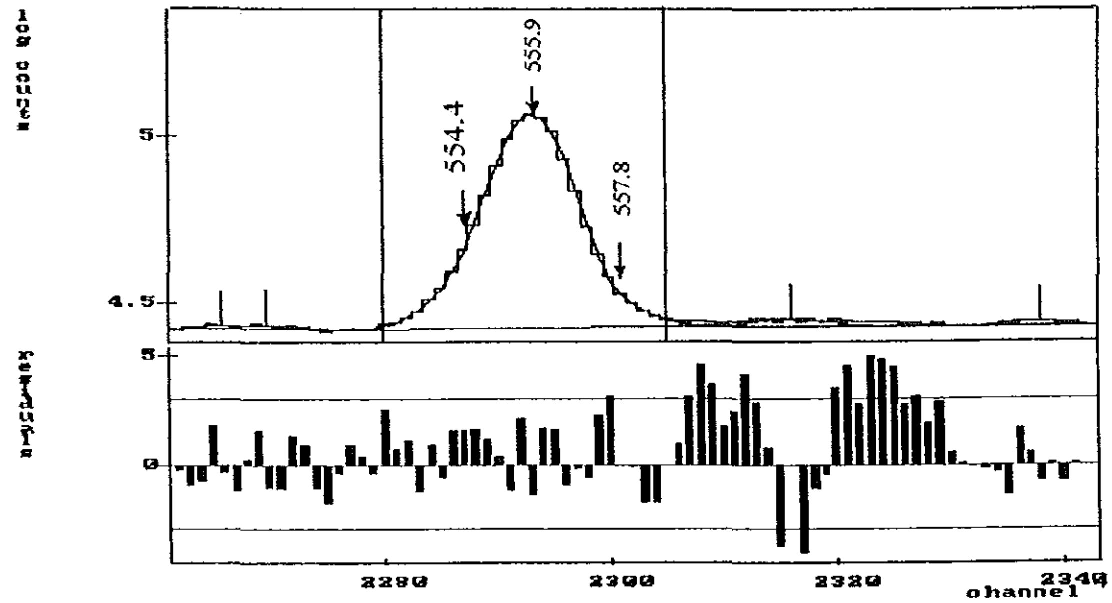

Fig. 4.11. Three peaks around 556 keV and the corresponding residuals.

B. The Nuclei ^{85,86}Kr

In our reaction the creation of the nucleus ^{85}Kr is accompanied by emission of one proton and three neutrons and ^{86}Kr by emission of one proton and two neutrons (see table 4.1). To study the excited states of these nuclei proton-gated coincidence measurements were done recently by Winter et al. [Win93] in order to suppress reaction channels with pure neutron evaporation. Based on these measurements excited states up to 4.8 MeV that are built on the ground state (spin $9^+/2$) and on top of the $17^+/2$ μs isomer at 1991.8 keV could be identified in the ^{85}Kr level scheme. For ^{86}Kr excited states up to 7.9 MeV have been observed.

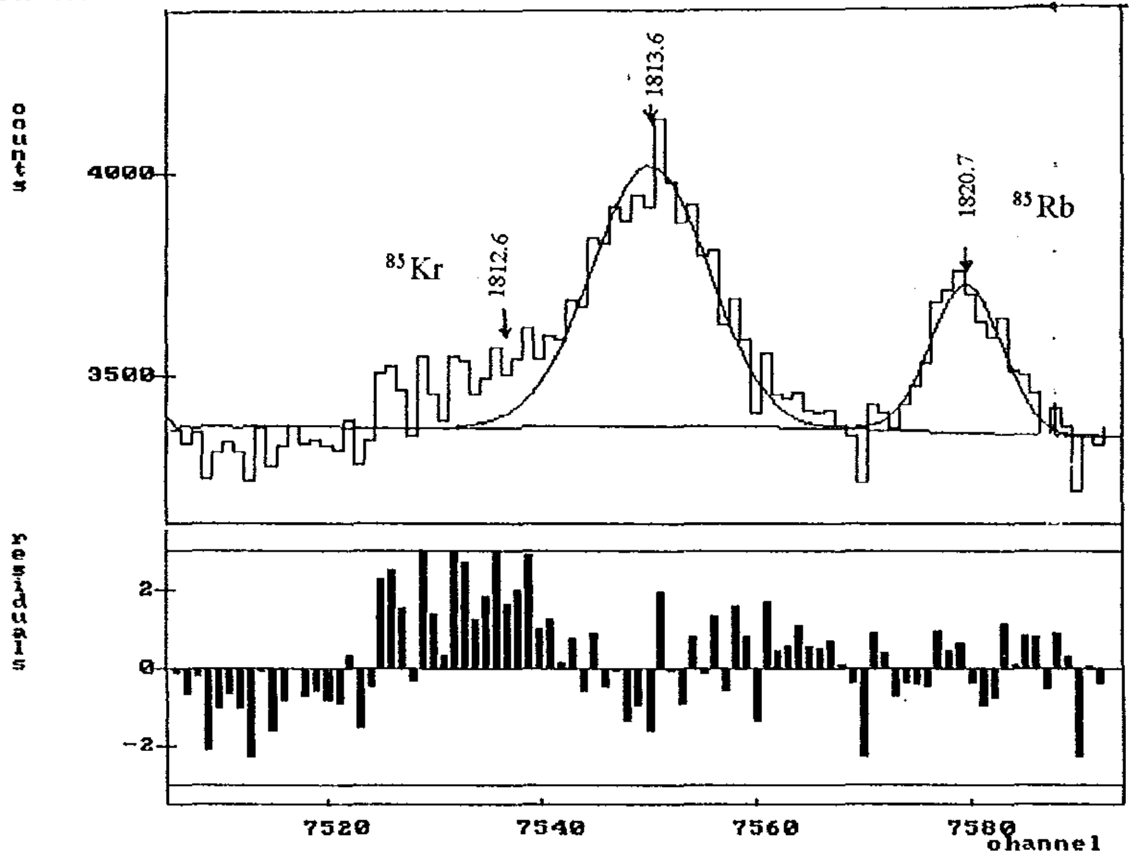

Fig. 4.14. The residuals give a clue that the low intensity 1812.6 keV peak is hidden in the more prominent 1814.1 keV line from ^{86}Kr, while the 1820.7 keV line from ^{85}Rb is not deformed by neighbouring lines.

In table 4.4 it is shown that most of the ^{85}Kr lines are seen by GANAAS in the singles spectrum. All lines (319.9, 1611.6 and 1931.6 keV) that are built on the ground state and most of the lines (except the 342.4, 1812.6 and 679.2 keV lines having low intensities) that are built on top of the 1991.8 keV isomer are found in the singles spectrum.

We mention the situation for one low-intensity transition. As seen from the residual of the line (see Fig. 4.14) the 1812.6 keV peak is hidden in the neighbouring prominent 1814.1 keV γ-line from ^{86}Kr.

As already discussed in the beginning of this section at lower γ-energies the relative intensities obtained are too large. This fact can be demonstrated with the help of a low energy interval shown in Fig. 4.15. As can be seen from the residuals obviously several lines are hidden in each peak. This results in an artificially increased intensity of the lines identified by GANAAS. Due to this fact the 60.3 keV line from ^{85}Kr has too large relative intensity. The same argument is also true for other low energy peaks or, in general, where the density of γ-transitions is too high.

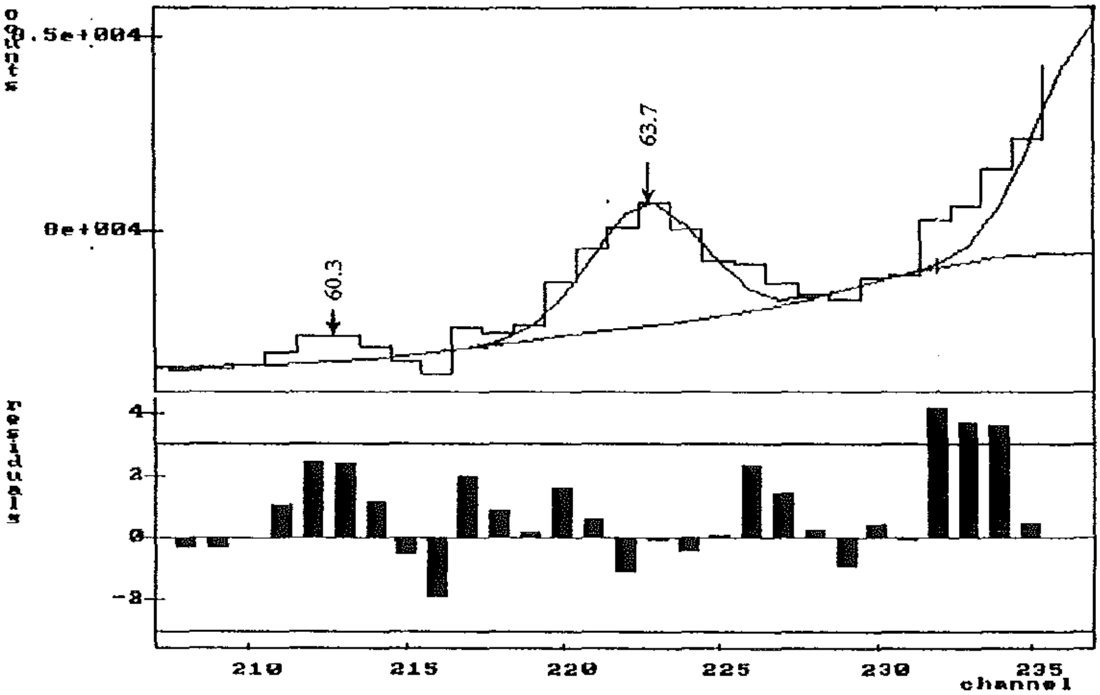

Fig. 4.15. Illustration of the difficulties faced by GANAAS at lower energies. Several lines are hidden in the energy interval shown. Therefore the intensity, for instance, of the 60.3 keV line in ^{85}Kr comes out too large.

As far as the lines in the level scheme of ^{86}Kr are concerned at energies above ~ 1000 keV there are some unseen lines of low relative intensities. To see such low intensity lines measurements in the γ-γ or γ-particle coincidence modes have to be done. The energies of the lines that are obtained with GANAAS are in a good agreement with the experimental values obtained by Winter et al. [Win93]. However, for the 262.8, 416.9 and 691.6 keV lines in ^{86}Kr a shift of about 1 keV to the lower or higher direction is obtained in our result (see table 4.5). The reason for this is the overlapping of different lines resulting in a bad fit quality for these lines (see table 4.5).

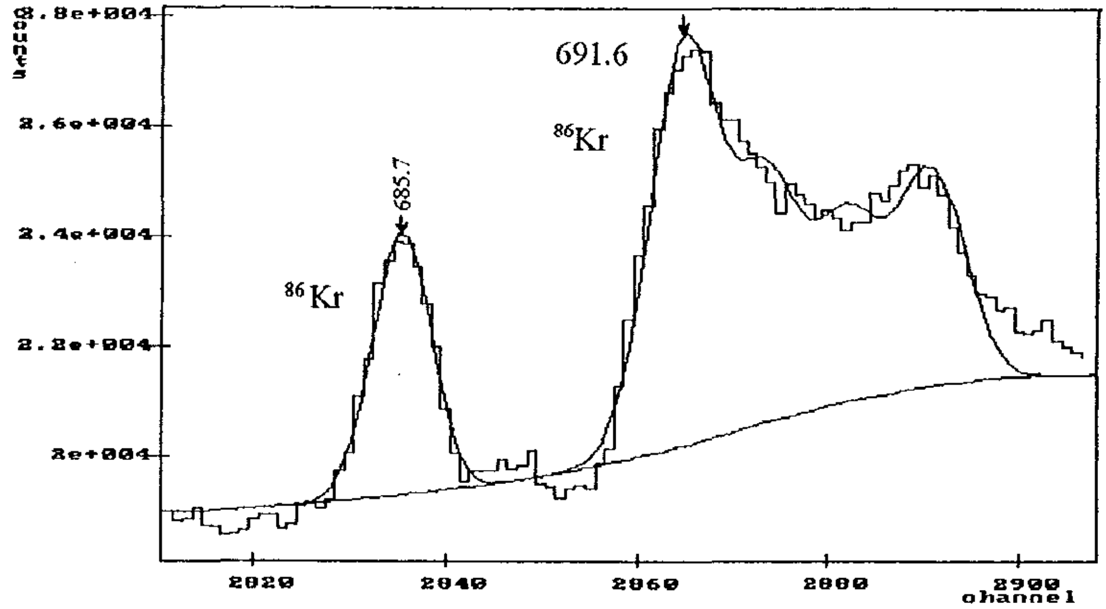

Fig. 4.16. Part of the fitted spectrum between ~ 680 keV to ~700 keV. Only for an isolated peak the correct energy is obtained. When the lines are overlapping the fit is always bad and the correct energy values can not be reproduced.

For example, in the energy region around 690 keV shown in Fig. 4.16 different lines are strongly overlapping, and therefore the fit result is bad leading to energy shifts of about 1 keV. On the other hand, for the relatively isolated 685.3 keV line from ^{86}Kr the fit quality is good, therefore the correct energy is reproduced by GANAAS.

Conclusions

In this work the singles spectrum measured at 90° of the ^{7}Li + ^{82}Se fusion-evaporation reaction is analyzed and the results of the analysis is compared with published data taken in coincidence mode. The analysis is done with the help of a special nuclear analysis software - Gamma spectrum Analysis, Activity calculations and Neutron Activation Analysis (GANAAS).

The GANAAS software package was developed under the control of the IAEA to carry out neutron activation, X-ray, Mössbauer spectrum analysis, etc. where one deals with a few isolated γ-or X-lines. In γ-spectra obtained from in-beam measurements using fusion-evaporation reactions several hundreds of γ-lines appear. This work was also aimed at checking if GANAAS is appropriate to analyze such complex spectra. Though the singles spectrum is a contribution of γ-lines from the isotopes Rb, Kr, Se, and Br, the nuclei chosen for a detailed analysis were ^{85,86}Rb and ^{85,86}Kr.

The results of the analysis show that the energies of the γ-lines obtained are in a quite good agreement with those of published data. However, some of the expected lines could not be identified because of their low intensities. These lines are found to be very weak transitions from side bands or highly excited states of the nuclear level schemes. The relative intensities obtained from the GANAAS fit have shown characteristic deviations from published data. From the pattern of the deviation it is supposed that agreement with published data can be obtained by correcting the data for the response function of the Ge-detector used.

Another possible source for the deviation might be the nature of the singles spectrum. At lower γ-energies, in general, where the transition density is high, the intensities of the lines are found too large since in this region many lines are hidden in one peak. Though the intensities are affected by different factors, the pattern of the relative intensities could be reproduced.

It should also be remembered that comparison is made between fitted data of a singles spectrum with those obtained with the help of multi-detector systems measuring γ-γ or particle-γ coincidences. In the latter case selection of a particular channel is possible and has been done. This reduces the complexity of the spectra, as a result the analysis will be easier. In the former case we have only a singles spectrum which is a combination of many reaction channels. Accordingly the analysis is also difficult. Therefore, with the limitations that can be done with a single detector and hence singles spectrum the result obtained is quite satisfactory. No question, GANAAS is a powerful γ-ray analysis software package when one deals with spectra having several tens of isolated γ-lines.

References

Aha85 D. P. Ahalpara et al, J. Phys. G: Nucl.Phys. **11**(1985)735

Alh93 Y. Alhassid, *Hot Rotating Nuclei*, in: Proc. Int. Nucl. Phys. Conf., Wiesbaden 1992, eds. R. Bock et al., Nucl. Phys. **A 553** (1993) 137c

Ari75 A. Arima and F. Iachello, Phys. Rev. Lett. **16** (1975) 1069; Ann. Phys. (N.Y.) 99 (1976) 253

Bak82 O. Bakander et al., Nucl. Phys. **A 389** (1982) 93

Boc89 R. Bock, *Heavy Ion Collisions*, Vol.2, North-Holland Pub. Comp., Amsterdam 1989

Boh69 A. Bohr and B. R. Mottelson, *Nuclear Structure*, Vol.1 W. A. Benjamin, New York, Amsterdam 1969

Bos81 R. V. Bosch and A. J. Lazzarini, Phys. Rev. **C 23** (1982) 1074

Buc83 D. Bucurescu et al., Nucl. Phys. **A 401** (1983) 22

Cha83 R. Champan et al., Phys. Rev. Lett. **51** (1983) 2265

Daw63 A. S. Dawydow, *Theory of the Atomic Nucleus*, Deutscher Verlag der Wissenschaften, Berlin 1963.

Dew82 A. Dewald et al., Phys. Rev. **C 26** (1982) 226

Dia86 R. M. Diamond, *High-Spin Nuclear Spectroscopy*, in: Proc. of the IX Workshop in Nucl. Phys., World Scientific, Buenos Aires 1986

Doe93 J. Döring et al., Phys. Rev. **C 47** (1993) 2560

Doe94 J. Döring et al., Phys. Rev. **C 49** (1994) 2419

Eas87 D. A. Eastham , Phys. Rev. **C 36** (1987) 1583

Ebe93 J. Eberth, Phys. Bl. **49** (1993) 1016

Fei81 R. A. Faires, G. G. J. Boswell, *Radiation Laboratory Techniques*, Butterworth & Co. Ltd., Boston 1981

Fen 83 Proc. Workshop on Bosons in Nuclei, ed. D.H.Feng et al., Drexel 1993, World Scientific 1989

Fen 86 T. Fenyes, *New experimental in-beam γ-and e^- - spectroscopic studies*, in: Nuclear Structure, Reactions and Symmetries, eds. R.A. Meyer and V.Paar, World Scientific, Vol.2, Dubrovnik 1986

Gal86 J. Galerin et al., J. Phys. G: Nucl. Phys. **12** (1986)329

Gal74 J. Galin et al., Phys. Rev. **C 9** (1974) 1018

Gar94 G. Garcia Burmunder et al., Phys. Rev. **C 49** (1994) 3309

Gar85 J. D. Garretta, *Spectroscopy of Rapidly Rotating Nuclei*, in: Proc. of a NATO Advanced Studies Institute International Summer School on New Vistas in Nuclear Dynamics, eds. P. J. Brussaard and J. H. Koch, Plenum Press, New York 1985

Ger92 EUROBALL III, European γ–ray facility, eds. J. Gerland, R.Lieder, Darmstadt 1992

Ghu94 S. S. Ghugre et al., Phys. Rev. C **50** (1994)1346

Gro67a J. R. Grover, Phys. Rev. **127** (1967) 814

Gro67b J. R. Grover, Phys. Rev. **127** (1967) 823

Hee94 J. Hees et al., Phys. Rev. C **49** (1994) 1896

Jaa83 M. Jaaskelainen et al., Nucl. Instrum. Meth. **204** (1983) 385

Joh75 A.Johnson, *Nuclear Rotation at High Angular Velocities*, in: Heavy-Ion High-Spin States and Nuclear Structure Vol.1, IAEA, Vienna 1975

Kau61 R. Kaufmann and R. Wolfgang, Phys. Rev. **121** (1961) 192

Kho78 T. C. Khoo et al., Phys. Rev. Lett. **41** (1978) 1027

Kie91 P. Kienle, *Directions of Heavy-Ion Physics*, Preprint GSI - 91- 03, Darmstadt 1991; Invited talk presented at the Yoshio Nishina Ceremonial Symp., Tokyo 1990

Lee80 S. M. Lee, Phys. Rev. Lett. **45** (1980) 165

Lee84 S. M. Lee et al., *Effects of Successive Critical Distances in Heavy Ion Fusion Reactions*, in: Heavy-ion fusion reactions, Proc. of the Tsukuba International Symp., eds. K. Furuno and T. Kishimoto, World Scientific 1984

Lie86 K.P.Lieb, *Electromagnatic Moments of High-Spin States in Medium-Mass Nuclei*, in: Reactor Physics for Developing Countries and Nuclear Spectroscopy Research, World Scientific 1986

Mas93 S. G. Mashnik, preprint Dubna, JINR E4-93-77 (1993)

M0l81 P. Moller and J. R. Nix, Nucl. Phys. A **361** (1981) 117

Mol84 P. Moller et al., Phys. Scr. **29** (1984) 402

Mos81 U. Mosel, *A Review of Heavy-Ion Fusion*, in: Proc. of the 3rd Adriatic Europhysics Conf. on the Dynamics of Heavy-Ion Collisions, ed. N.Cindro et al., North-Holland, New York 1981

Man91 Manual of GANAAS, IAEA,Vienna 91

Naz85 W. Nazarewicz et al., Nucl. Phys. A **435** (1985) 397

Pel82 D. Pelte and D. Schwalm, *In-Beam Gamma-Ray Spectroscopy*, in: Heavy ion collisions, Vol.3, ed. R. Bock, North-Holland 1982

Puh77 W. Puhlhofer, Nucl. Phys. A **280** (1977) 267

Rei93 J. Reif et al., Annual report 1993, Institute of Nuclear and Hadron Physics, Forschungszentrum Rossendorf

Sch91 R. Schwengner et al., Annual reports 1991 and 1993, Institute of Nuclear and Hadron Physics, Forschungszentrum Rossendorf

Sch93 R. Schwengner et al., Institute of Nuclear and Hadron Physics, Forschungszentrum Rossendorf 1993

Sie75 P. J. Siemens, *A First orientation in Heavy-Ion Reactions*, in: Heavy-Ion High-Spin States and Nuclear Structure, Vol.1, IAEA, Vienna 1975

Tri94 K. C. Tripathy and R. Sahn, J. Phys. G: Nucl. Phys. **20** (1994) 911

Twi83 P. J. Twin, Nuclear Physics A **409** (1983) 343c-352c

Twi86 P. J. Twin et al, Phys. Rev. Lett. **57** (1986) 811

Twi89 P. J. Twin, *The Evolution of Nuclear Structure at High-Spin*, in: Proc. Int. School of Physics, ed. P. Kienle et al., North-Holland 1989

Twi94 P. J. Twin, in: Proc. Conf. on Perspectives in Nuclear Structure, Copenhegen 1993, ed. J. J. Gaardhoge, Herskind, I. Hamamoto, B. Mottelson and A. Winther, Nucl. Phys. A **574** (1994) No. 1, 2

Voi83 M.J.A de Voigt et al., Rev. Mod. Phys. **55** (1983) 949

Win89 G.Winter et al., Z.Phys. A **334** (1989) 415

Win93 G.Winter et al., Phys, Rev. C **48** (1993) 1010

Win94 G.Winter et al., Phys. Rev. C **49** (1994) 2427

Appendix

Energy calibration data and results of spectrum analysis

Table. A1. Energy calibration data.

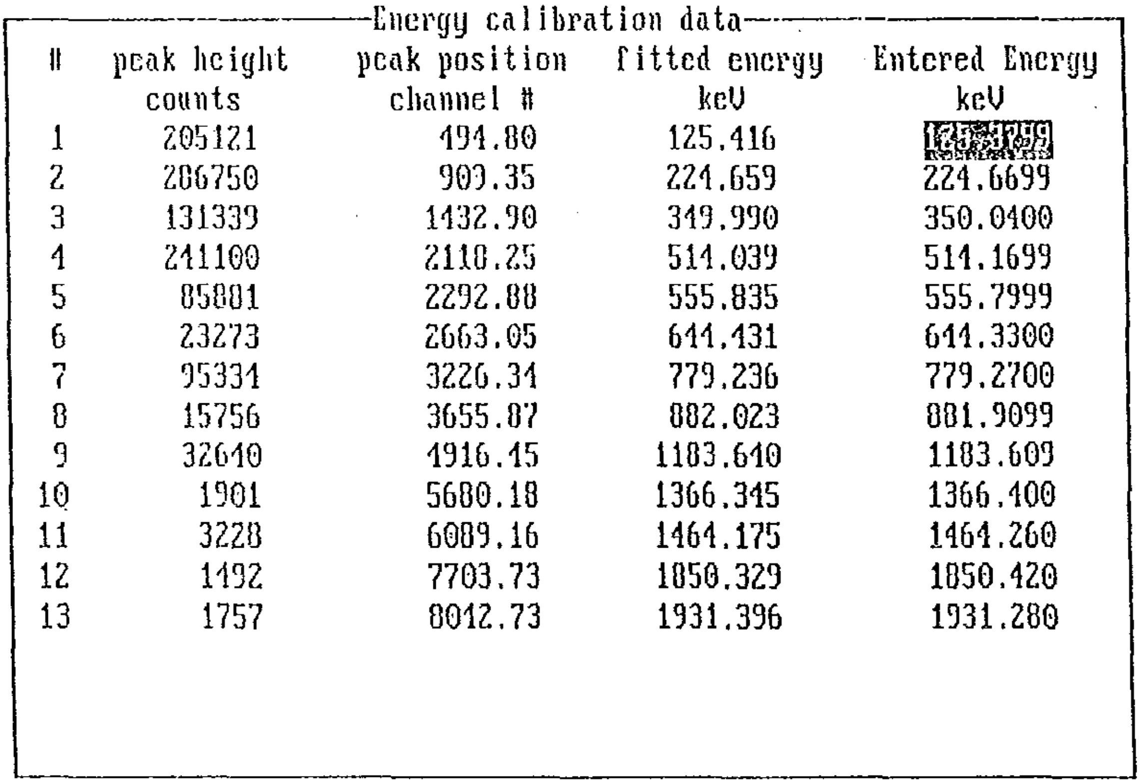

```
─────────────────Energy calibration data─────────────────────
 #   peak height   peak position  fitted energy  Entered Energy
       counts        channel #         keV            keV
 1     205121          494.80        125.416        125.3799
 2     206750          909.35        224.659        224.6699
 3     131339         1432.90        349.990        350.0400
 4     241100         2110.25        514.039        514.1699
 5      85801         2292.88        555.835        555.7999
 6      23273         2663.05        644.431        644.3300
 7      95331         3226.34        779.236        779.2700
 8      15756         3655.87        882.023        881.9099
 9      32640         4916.15       1183.640        1183.609
10       1901         5680.18       1366.345        1366.400
11       3228         6089.16       1464.175        1464.260
12       1492         7703.73       1850.329        1850.420
13       1757         8012.73       1931.396        1931.280
```

Table. A2. Results of spectrum analysis.

PEAK#	CHANNEL	FWHM [keV]	ENERGY [keV]	AREA [counts]	QUALITY OF FIT
1	165.83	0.977	46.66	14621 ± 2827	2.00
2	194.92	0.991	53.62	91788 ± 8023	23.00
3	201.13	0.991	55.11	6230 ± 4538	10.00
4	222.74	1.008	60.28	15810 ± 2444	1.00
5	237.14	1.015	63.73	27849 ± 3109	3.00
6	241.94	1.015	64.88	19359 ± 3467	6.00
7	248.68	1.015	66.49	30982 ± 3419	6.00
8	261.60	1.029	69.58	25190 ± 4757	6.00
9	269.07	1.029	71.37	30602 ± 5615	9.00
10	284.84	0.879	75.15	6389 ± 1802	1.00
11	294.25	1.049	77.40	16866 ± 2449	1.00
12	304.83	1.049	79.93	65276 ± 5896	4.00
13	308.12	1.049	80.72	147398 ± 8041	7.00
14	317.34	1.049	82.93	37644 ± 5290	9.00
15	321.35	1.049	83.89	160694 ± 6967	13.00
16	340.25	1.070	88.41	12010 ± 2368	1.00
17	374.74	0.546	96.67	2585 ± 1442	1.00
18	388.95	1.096	100.07	19835 ± 3713	2.00
19	393.54	1.096	101.17	61164 ± 5040	4.00
20	415.99	1.108	106.55	52137 ± 4666	3.00
21	419.78	1.108	107.45	166039 ± 6062	6.00
22	427.36	1.108	109.27	38092 ± 6479	3.00
23	430.94	1.108	110.12	82388 ± 5713	2.00
24	445.35	1.123	113.57	21316 ± 3526	2.00
25	467.62	0.716	118.90	5184 ± 1947	1.00
26	482.13	1.142	122.38	46373 ± 5031	1.00
27	485.53	1.142	123.19	71862 ± 5444	1.00
28	491.79	1.142	124.69	180648 ±17746	2.00
29	494.87	1.142	125.43	747625 ±47853	1.00
30	496.76	1.142	125.88	402964 ±53420	1.00
31	511.11	1.156	129.32	202521 ±15737	19.00
32	514.61	1.156	130.15	540870 ±19030	25.00
33	537.91	1.168	135.73	26978 ± 3816	2.00
34	555.70	1.175	139.99	35791 ± 4655	3.00
35	574.31	1.185	144.44	46471 ± 2763	1.00
36	597.44	1.195	149.98	45932 ± 6869	20.00
37	602.67	1.195	151.23	367583 ±11304	29.00
38	610.78	1.195	153.18	23505 ± 6663	11.00
39	615.46	1.195	154.30	39467 ± 4528	4.00
40	623.46	1.195	156.21	40950 ± 2957	2.00
41	635.61	1.214	159.12	23794 ± 2860	2.00
42	677.99	1.230	169.27	41086 ± 2713	1.00
43	704.81	1.221	175.69	30074 ± 2290	1.00
44	727.12	1.254	181.03	13156 ± 3312	2.00
45	732.46	1.254	182.30	35413 ± 4461	6.00
46	740.29	1.254	184.18	151156 ± 5640	10.00
47	746.28	1.254	185.61	30670 ± 4334	7.00

PEAK#	CHANNEL	FWHM [keV]	ENERGY [keV]	AREA [counts]	QUALITY OF FIT
1	769.05	1.271	191.06	84629 ±10305	51.00
2	775.92	1.271	192.71	413837 ±21266	77.00
3	783.36	1.271	194.49	31319 ± 8574	41.00
4	794.72	1.271	197.21	155454 ± 9768	33.00
5	825.31	1.297	204.53	10280 ± 2235	1.00
6	838.62	1.302	207.72	35076 ± 4243	2.00
7	867.42	1.266	214.61	32172 ± 4118	1.00
8	872.02	1.266	215.71	79787 ± 4022	1.00
9	877.97	1.266	217.14	29343 ± 3797	1.00
10	905.10	1.329	223.63	260186 ±22233	4.00
11	908.45	1.329	224.43	1412720 ±15246	5.00
12	912.19	1.329	225.33	913228 ±21442	4.00
13	921.24	1.329	227.50	176794 ± 7752	2.00
14	924.55	1.329	228.29	839622 ± 8197	2.00
15	952.15	1.132	234.90	9071 ± 1776	1.00
16	987.09	1.362	243.26	35142 ± 3291	2.00
17	993.40	1.362	244.77	44519 ± 3258	2.00
18	1002.61	1.362	246.97	25666 ± 3355	2.00
19	1007.45	1.362	248.13	277624 ± 3807	1.00
20	1050.46	1.388	258.43	11707 ± 1956	1.00
21	1058.86	1.388	260.44	44292 ± 3357	3.00
22	1072.46	1.388	263.69	69388 ± 5363	11.00
23	1095.14	1.405	269.12	51713 ± 3669	1.00
24	1123.95	1.417	276.02	79670 ± 2769	1.00
25	1137.66	1.417	279.30	14590 ± 2100	1.00
26	1166.74	1.434	286.26	6940 ± 1672	1.00
27	1173.58	1.434	287.90	23414 ± 1861	1.00
28	1184.40	1.434	290.49	81655 ± 2409	2.00
29	1202.66	1.441	294.86	18954 ± 1841	1.00
30	1239.42	1.460	303.66	107444 ± 4210	3.00
31	1253.44	1.460	307.01	54306 ± 3292	4.00
32	1272.31	1.472	311.53	32722 ± 2437	1.00
33	1287.91	1.479	315.27	7137 ± 1897	1.00
34	1305.55	1.486	319.49	9996 ± 1897	1.00
35	1313.80	1.486	321.46	48034 ± 1992	1.00
36	1351.59	1.503	330.51	58197 ± 5208	3.00
37	1356.45	1.503	331.67	222595 ± 7043	6.00
38	1375.00	1.513	336.11	10302 ± 1852	1.00
39	1408.32	1.218	344.09	9205 ± 1494	1.00
40	1429.03	1.510	349.04	90455 ±10329	1.00
41	1432.91	1.510	349.97	834559 ± 6501	1.00
42	1436.86	1.510	350.92	93068 ± 9855	1.00
43	1454.49	1.539	355.14	79398 ± 4340	5.00
44	1461.54	1.539	356.83	1021287 ± 6645	3.00
45	1484.62	1.161	362.35	4848 ± 1411	1.00

PEAK#	CHANNEL	FWHM [keV]	ENERGY [keV]	AREA [counts]	QUALITY OF FIT
1	1504.84	1.558	367.19	14294 ± 2058	1.00
2	1524.84	1.565	371.98	17073 ± 1992	1.00
3	1544.77	1.573	376.75	63161 ± 2396	1.00
4	1566.30	1.580	381.90	12947 ± 2396	1.00
5	1601.09	1.592	390.23	31110 ± 2568	1.00
6	1640.53	1.606	399.67	10758 ± 2046	2.00
7	1652.27	1.606	402.48	19681 ± 2144	2.00
8	1673.34	1.616	407.52	69275 ± 6042	5.00
9	1708.70	1.628	415.99	19396 ± 4320	3.00
10	1732.55	1.637	421.70	18547 ± 1895	1.00
11	1747.88	1.637	425.37	147826 ± 3887	3.00
12	1759.95	1.637	428.25	45452 ± 2024	1.00
13	1781.44	1.620	433.40	18559 ± 1631	1.00
14	1793.02	1.620	436.17	49874 ± 1662	1.00
15	1808.06	1.663	439.77	11709 ± 1535	1.00
16	1837.56	1.671	446.83	18435 ± 3016	4.00
17	1848.79	1.671	449.52	37649 ± 3930	6.00
18	1856.41	1.671	451.34	42350 ± 4388	9.00
19	1869.88	1.671	454.57	34995 ± 3825	8.00
20	1882.05	1.671	457.48	22513 ± 2968	4.00
21	1909.02	1.692	463.93	64934 ± 2171	1.00
22	1929.74	1.702	468.89	15042 ± 3303	4.00
23	1956.74	0.862	475.36	3269 ± 1021	1.00
24	1973.59	1.714	479.39	67177 ± 3828	2.00
25	2001.51	0.967	486.07	2596 ± 932	1.00
26	2051.17	1.738	497.96	30789 ± 3072	1.00
27	2103.19	1.623	510.41	519209 ±54015	1.00
28	2109.68	1.623	511.96	613822 ±250205	3.00
29	2118.98	1.623	514.19	1932930 ±197975	6.00
30	2133.77	1.623	517.73	28050 ± 4518	3.00
31	2186.52	1.781	530.35	42372 ± 2792	2.00
32	2197.84	1.781	533.06	8590 ± 1660	1.00
33	2212.17	1.781	536.49	30762 ± 2236	1.00
34	2228.89	1.795	540.49	21660 ± 2097	2.00
35	2241.08	1.795	543.41	33583 ± 2842	6.00
36	2267.93	1.654	549.84	5668 ± 1442	1.00
37	2287.13	1.694	554.43	62925 ± 2317	1.00
38	2293.23	1.694	555.89	666188 ± 4421	2.00
39	2301.09	1.694	557.77	27089 ± 2106	2.00
40	2315.84	1.694	561.30	12248 ± 2263	5.00
41	2338.18	1.510	566.65	7260 ± 1347	1.00
42	2361.55	1.836	572.24	46517 ± 2031	1.00
43	2378.88	1.840	576.39	15736 ± 2202	1.00
44	2405.43	1.848	582.75	72905 ± 2657	1.00
45	2412.95	1.848	584.54	11437 ± 2616	1.00
46	2451.10	1.089	593.68	2243 ± 1037	1.00
47	2463.81	1.867	596.72	37553 ± 5580	6.00
48	2476.23	1.867	599.69	18002 ± 3699	7.00

PEAK#	CHANNEL	FWHM [keV]	ENERGY [keV]	AREA [counts]	QUALITY OF FIT
1	2517.70	1.881	609.61	171808 ± 3759	3.00
2	2538.62	1.881	614.62	49082 ± 2846	6.00
3	2547.19	1.881	616.67	48029 ± 2384	3.00
4	2559.72	1.881	619.67	33899 ± 2131	2.00
5	2570.22	1.881	622.18	85080 ± 2894	6.00
6	2602.58	1.905	629.93	20007 ± 2673	1.00
7	2609.04	1.905	631.48	25115 ± 2681	1.00
8	2632.12	1.915	637.00	5908 ± 1472	1.00
9	2656.74	1.922	642.89	26678 ± 3095	1.00
10	2663.13	1.922	644.42	199398 ± 3001	1.00
11	2669.97	1.922	646.06	23838 ± 2960	1.00
12	2707.34	1.845	655.00	135465 ± 2325	3.00
13	2738.69	1.943	662.50	55754 ± 4246	5.00
14	2755.42	1.943	666.51	25548 ± 2930	6.00
15	2787.97	1.376	674.30	3023 ± 1074	1.00
16	2835.41	1.891	685.65	44744 ± 3556	1.00
17	2865.41	1.982	692.83	86626 ± 7365	27.00
18	2876.66	1.982	695.52	59289 ± 6179	32.00
19	2889.00	1.982	698.47	61287 ± 5807	24.00
20	2901.60	1.982	701.49	28337 ± 3807	16.00
21	2918.38	1.982	705.50	20577 ± 3034	10.00
22	2947.06	1.685	712.37	7006 ± 1205	1.00
23	2973.10	1.692	718.60	26537 ± 1495	1.00
24	2996.20	2.015	724.13	20167 ± 2526	1.00
25	3015.00	1.012	728.63	1838 ± 667	1.00
26	3033.52	2.027	733.06	135086 ± 4509	5.00
27	3045.04	2.027	735.82	23854 ± 2376	5.00
28	3098.78	2.044	748.68	9892 ± 1395	1.00
29	3113.67	2.048	752.24	22469 ± 1924	1.00
30	3183.39	2.068	768.92	18694 ± 1618	2.00
31	3193.68	2.068	771.39	17892 ± 1597	2.00
32	3219.28	2.029	777.51	130437 ± 6977	9.00
33	3227.30	2.029	779.43	902351 ± 6307	9.00
34	3240.32	2.029	782.55	13213 ± 3455	2.00
35	3288.98	2.096	794.19	8150 ± 1322	1.00
36	3311.69	1.797	799.63	28710 ± 1094	1.00
37	3324.14	1.797	802.61	4992 ± 1077	1.00
38	3340.88	2.108	806.61	9953 ± 1449	1.00
39	3359.96	1.560	811.18	9470 ± 1126	1.00
40	3394.80	2.123	819.52	10028 ± 1421	1.00
41	3430.35	2.130	828.02	27999 ± 2055	1.00
42	3460.41	2.139	835.22	45058 ± 2831	1.00
43	3470.38	2.139	837.60	16687 ± 2603	1.00
44	3497.69	1.931	844.14	25562 ± 1240	1.00
45	3510.26	1.931	847.15	16642 ± 1211	1.00
46	3527.57	1.467	851.29	3141 ± 1154	1.00
47	3589.40	2.173	866.08	76426 ± 3616	7.00
48	3598.49	2.173	868.26	58228 ± 3702	8.00
49	3607.70	2.173	870.46	22139 ± 3216	4.00

PEAK#	CHANNEL	FWHM [keV]	ENERGY [keV]	AREA [counts]	QUALITY OF FIT
1	3655.86	2.027	881.99	146819 ± 3117	3.00
2	3730.96	1.106	899.96	1890 ± 655	1.00
3	3747.72	1.986	903.97	19617 ± 1387	1.00
4	3765.88	1.108	908.31	1892 ± 597	1.00
5	3877.34	2.151	934.98	13752 ± 2098	1.00
6	3888.10	2.151	937.56	49868 ± 2108	1.00
7	3945.42	2.261	951.27	12414 ± 1295	1.00
8	4013.57	1.464	967.58	3481 ± 856	1.00
9	4040.27	2.283	973.97	11216 ± 1423	1.00
10	4084.07	2.156	984.45	5502 ± 1146	1.00
11	4101.22	1.895	988.55	9169 ± 1028	1.00
12	4132.85	1.802	996.12	6373 ± 1013	1.00
13	4160.67	1.900	1002.78	28312 ± 1508	1.00
14	4210.03	2.280	1014.59	185303 ± 2543	2.00
15	4220.00	2.280	1016.98	10986 ± 2032	1.00
16	4279.64	2.340	1031.24	21688 ± 2328	3.00
17	4330.08	2.350	1043.31	29639 ± 4364	9.00
18	4380.03	2.283	1055.27	5375 ± 1000	1.00
19	4419.30	2.371	1064.66	56667 ± 2110	1.00
20	4447.52	1.840	1071.41	5186 ± 943	1.00
21	4474.89	2.385	1077.96	27959 ± 1099	1.00
22	4491.34	2.385	1081.90	17834 ± 1346	3.00
23	4502.13	2.385	1084.48	5920 ± 1198	2.00
24	4550.90	1.816	1096.15	6068 ± 973	1.00
25	4566.03	1.335	1099.77	2423 ± 777	1.00
26	4633.58	1.998	1115.93	9909 ± 1050	1.00
27	4658.11	1.651	1121.80	3516 ± 785	1.00
28	4669.56	2.431	1124.54	5785 ± 1043	1.00
29	4826.48	2.464	1162.08	6836 ± 957	1.00
30	4876.36	2.273	1174.02	13086 ± 1235	1.00
31	4889.19	2.273	1177.09	26421 ± 1298	1.00
32	4903.58	2.273	1180.53	13219 ± 1286	1.00
33	4916.50	2.273	1183.62	351200 ± 3645	5.00
34	4951.43	2.074	1191.98	3781 ± 925	1.00
35	5043.59	2.457	1214.03	32902 ± 1198	1.00
36	5061.48	2.457	1218.31	9968 ± 1135	1.00
37	5127.73	2.531	1234.16	34108 ± 3426	2.00
38	5175.08	2.543	1245.48	3497 ± 971	1.00
39	5240.02	2.309	1261.02	6839 ± 1079	1.00
40	5295.74	2.438	1274.35	5545 ± 903	1.00
41	5337.54	2.270	1284.35	13479 ± 1003	1.00
42	5353.93	2.100	1288.27	3782 ± 863	1.00
43	5455.86	2.201	1312.66	3027 ± 877	1.00
44	5478.50	2.455	1318.07	11030 ± 1148	1.00
45	5530.32	2.268	1330.47	2468 ± 862	1.00
46	5540.78	2.268	1332.97	11970 ± 809	1.00
47	5609.96	1.902	1349.52	3577 ± 816	1.00
48	5624.98	2.167	1353.12	4383 ± 848	1.00

PEAK#	CHANNEL	FWHM [keV]	ENERGY [keV]	AREA [counts]	QUALITY OF FIT
1	5680.22	2.471	1366.33	22808 ± 1591	1.00
2	5709.54	1.328	1373.34	1241 ± 505	1.00
3	5790.44	2.359	1392.70	25416 ± 1056	1.00
4	5968.76	2.397	1435.36	5767 ± 872	1.00
5	6010.33	2.158	1445.30	7580 ± 1125	1.00
6	6048.49	2.725	1454.43	17483 ± 1450	1.00
7	6089.42	2.643	1464.22	41092 ± 1779	2.00
8	6135.07	2.076	1475.14	3052 ± 709	1.00
9	6422.40	2.299	1543.87	5142 ± 814	1.00
10	6511.25	2.672	1565.12	21419 ± 770	1.00
11	6529.10	2.672	1569.39	17949 ± 780	1.00
12	6542.83	2.672	1572.68	3818 ± 788	1.00
13	6650.99	2.842	1598.55	23106 ± 1378	1.00
14	6707.19	2.466	1611.99	5016 ± 698	1.00
15	6719.81	2.466	1615.01	1663 ± 692	1.00
16	6799.72	2.815	1634.12	4616 ± 822	1.00
17	7018.06	1.457	1686.35	1621 ± 442	1.00
18	7038.79	2.693	1691.30	3977 ± 776	1.00
19	7401.72	1.830	1778.11	2022 ± 584	1.00
20	7408.16	1.830	1779.65	3483 ± 578	1.00
21	7550.27	3.011	1813.64	9586 ± 1490	1.00
22	7579.98	2.248	1820.74	3916 ± 684	1.00
23	7703.74	3.028	1850.34	23392 ± 2223	1.00
24	7834.95	3.064	1881.72	4517 ± 757	1.00
25	7899.00	3.073	1897.04	6062 ± 898	1.00
26	7951.57	2.071	1909.61	2709 ± 568	1.00
27	8042.78	3.087	1931.42	26785 ± 1078	1.00